INVESTIGATION OF FLUID RHEOLOGY EFFECTS ON ULTRASOUND PROPAGATION

A THESIS SUBMITTED TO
THE GRADUATE SCHOOL AND APPLIED SCIENCES
OF
MIDDLE EAST TECHNICAL UNIVERSITY

BY

OKAN ÖZKÖK

IN PARTIAL FULFILLMENT OF THE REQUIREMENTS
FOR
THE DEGREE OF MASTER OF SCIENCE
IN
CHEMICAL ENGINEERING

SEPTEMBER 2012

Approval of the thesis:

INVESTIGATION OF FLUID RHEOLOGY EFFECTS ON ULTRASOUND PROPAGATION

submitted by **OKAN ÖZKÖK** in partial fulfillment of the requirements for the degree of **Master of Science in Chemical Engineering Department, Middle East Technical University** by,

Prof. Dr. Canan Özgen _____
Dean, Graduate School of **Natural and Applied Sciences**

Prof. Dr. Deniz Üner _____
Head of Department, **Chemical Engineering**

Assoc. Prof. Dr. Yusuf Uludağ _____
Supervisor, **Chemical Engineering Dept., METU**

Examining Committee Members:

Prof. Dr. Göknur Bayram _____
Chemical Engineering Dept., METU

Prof. Dr. Levent Yılmaz _____
Chemical Engineering Dept., METU

Prof. Dr. Ahmet Nedim Eraslan _____
Engineering Sciences Dept., METU

Assoc. Prof. Dr. Halil Kalıpçılar _____
Chemical Engineering Dept., METU

Assoc. Prof. Dr. Yusuf Uludağ _____
Chemical Engineering Dept., METU

Date: _____

I hereby declare that all information in this document has been obtained and presented in accordance with academic rules and ethical conduct. I also declare that, as required by these rules and ethical conduct, I have fully cited and referenced all material and results that are not original to this work.

Name, Last Name: Okan Özkök

Signature:

ABSTRACT

INVESTIGATION OF FLUID RHEOLOGY EFFECTS ON ULTRASOUND PROPAGATION

Özkök, Okan

M.S., Department of Chemical Engineering

Supervisor: Assoc. Prof. Dr. Yusuf Uludağ

September 2012, 87 pages

In this study, a mathematical model is developed for investigating the discrete sound propagation in viscoelastic medium to identify its viscoelastic properties. The outcome of the model suggests that pulse repetition frequency is a very important parameter for the determination of relaxation time. Adjusting the order of magnitude of the pulse repetition frequency, the corresponding relaxation time which has similar magnitude with pulse repetition frequency is filtered while the others in the spectrum are discarded. Discrete relaxation spectrum can be obtained by changing the magnitude of the pulse repetition frequency. Therefore, the model enables to characterize the relaxation times by ultrasonic measurements.

Keywords: Fluid Rheology, Ultrasonic Characterization Techniques, Discrete Sound Signal Propagation, Viscoelasticity, Relaxation Time

ÖZ

AKIŞKAN REOLOJİSİNİN ULTRASON YAYILMASI ÜZERİNDEKİ ETKİLERİNİN İNCELENMESİ

Özkök, Okan
Yüksek Lisans, Kimya Mühendisliği Bölümü
Tez Yöneticisi: Doç. Dr. Yusuf Uludağ

Eylül 2012, 87 sayfa

Bu çalışmada viskoelastik özelliklerin tayini için, viskoelastik ortamda kesikli ses sinyallerinin yayılmasını inceleyen bir matematiksel modelleme geliştirildi. Modellemenin sonuçları, dalga tekrarlanma frekansının relaksiyon zamanının tayininde çok önemli bir ölçüt olduğunu vurgulamaktadır. Dalga tekrarlanma frekansının büyüklüğünün ayarlanmasıyla, bu büyüklüğe yakın büyüklükteki relaksiyon zamanı süzülür ve bu arada spektrumdaki diğer relaksiyon zamanları elenir. Bu, dalga tekrarlanma frekansının büyüklüğünün değiştirilmesiyle kesikli relaksiyon spektrumunun elde edilmesini sağlar. Böylece, geliştirilen model relaksiyon zamanlarının ultrason ölçümleriyle bulunmasını sağladı.

Anahtar Kelimeler: Akışkan Reolojisi, Ultrasonik Karakterizasyon Teknikleri, Kesikli Ses Sinyali Yayılımı , Viskoelastiklik, Relaksiyon Zamanı

To my family

ACKNOWLEDGEMENTS

I am very grateful to my supervisor Assoc. Prof. Dr. Yusuf Uludağ for his support and supervision during this study. Without his criticisms and guidance this study could not be completed.

I am very grateful to my friends and laboratory members Hasan Zerze, Tarık Yücel, Gökhan Çelik and Güler Bengüsu Tezel.

I would also like to express my gratitude my family for their endless support and help.

TABLE OF CONTENTS

LIST OF TABLES

LIST OF FIGURES

LIST OF SYMBOLS

A : amplitude of ultrasound wave, Helmholtz free energy

a : time between two consecutive pulses

c : speed of sound

C_V : specific heat capacity at constant volume

E : modulus of elasticity

E^* : complex modulus of elasticity

E’ : dynamic modulus of elasticity

E’’ : loss modulus of elasticity

e : base of natural logarithm

f : frequency

G : shear modulus

G^* : complex shear modulus

G’ : dynamic shear modulus

G’’ : shear loss modulus

i : $(-1)^{1/2}$

J : compliance

J^* : complex compliance

J’ : dynamic compliance

J’’ : loss compliance

K : bulk modulus

K_T : isothermal bulk modulus

L : longitudinal modulus of elasticity

L^* : complex longitudinal modulus of energy

L’ : dynamic longitudinal modulus of elasticity

L’’ : loss longitudinal modulus of elasticity

M : any type of modulus of elasticity

m : number of discrete waves sent to sample

n : duration of a pulse

P : ultrasonic pressure

P_{0k} : complex pressure amplitude

p : number of relaxation time governing the material

q_x : heat flux at the x direction

T : temperature, period of oscillation

T_{0k} : complex temperature amplitude

t : continuous time

u : displacement of particles

u_{0k} : complex displacement amplitude

u_{ik} : strain tensor

v : particle velocity

w : angular frequency

x : axial direction

Z : acoustic empedance

Abbreviations

CMC : carboxy methyl cellulose

PRF : pulse repetition frequency

UDV : ultrasound Doppler velocimetry

Greek Letters

γ : strain

$\dot{\gamma}$: shear rate

δ : phase shift

α : sound attenuation

α_V : thermal expansion coefficient

η : shear viscosity

η' : bulk viscosity

η_0 : zero shear viscosity

λ : wavelength

μ : viscosity

ρ : density

P_{0k} : complex density amplitude

σ : wave number

σ_{xx} : stress tensor

σ_{xy} : shear stress

τ : relaxation time

Subscripts

i : summation index

j : summation index

Superscripts

* : complex conjugate

Functions and Operators

H : Heaviside unit step function

Im( ) : imaginary part

Re ( ) : real part

CHAPTER 1

INTRODUCTION

Non-invasive methods for characterization of materials have been commonly used over the last decades since they have various superiorities on the conventional methods such as viscometer and rheometer [1]. Ultrasonic techniques are one of the most promising methods among them since they offer high confidence level results with fast measurements and at lower equipment and labor costs [2] compared to other techniques. In the ultrasonic techniques two parametric quantities are used for characterization of materials; ultrasound propagation speed and the attenuation. The latter corresponds to the decrease in the amplitude of sound due to the absorption and scattering [3]. Since, these parameters are strongly dependent on the material properties, they can be utilized to determine the structure and physical properties [4] of the materials, mobility of molecules [5], complex modulus of elasticity [6], phase transformations [7], specific heat, thermal conductivity and other thermophysical properties [8, 9].

In particular, ultrasonic methods are suitable for polymer processing since fast monitoring of the process is critical for the end product quality and economics of the production. Hence, there are various studies done for in-line and on-line monitoring of the process. In their study, P. Zhao and his fellow workers used online ultrasonic measurement method in order to probe viscoelastic properties of the polymers during injection molding [4]. Their measurements were based on the relation between polymer structure and attenuation of

ultrasound propagating in the polymer. Any change observed in the amplitude versus time plot was a direct indicator of the viscoelastic properties of the polymer throughout the process.

Acoustic methods can also be used for the investigation of phase morphology of polymers. Wang and co-workers studied the structure of the high density polyethylene/ polyamide 6 blend melts with the addition of compatibilizer [10]. They found that the sound speed changes linearly with the blend composition. In addition, an exponential increase in the sound attenuation was observed as compatibilizer concentration was increased. Therefore, the phase morphology of polymer blends during processing can be watched online by using the ultrasonic techniques [11]. Similarly, Silva et al. accomplished the microstructural characterization of different types of AISI steels [13]. Their results revealed that the sound speed changes according to the type of steel. The variation of the sound speeds between these phases is mainly due to different degree of lattice distortion that changes the modulus of elasticity of these phases.

Ultrasonic methods are also commonly applied for characterizing the crystallization behavior of polymers. In the research of Zhao and coworkers, the connection between crystallization process of poly(ethyleneterephthalate) and ultrasonic parameters were investigated [7]. Variation of attenuation and sound speed in polymer samples with respect to time and temperature resulted in significant data about the crystallization process, specifically rate of crystallization and degree of crystallinity.

Ultrasonic techniques can also be employed to determine the complex modulus of elasticity. In their work, Laura and co-workers [16] probed the complex modulus of elasticity of dough during its fermentation by the use of attenuation and sound speed. Since, the properties of the medium change during fermentation, the complex modulus of elasticity changes, as well. This makes it available to monitor the process online. Similar study is done by

Álvarez et al. [12] for the determination of complex modulus of elasticity of silica aerogels. Frequency dependent values of modulus of elasticity were evaluated. Increase in the storage component with frequency was observed.

Besides, many studies are done to investigate the viscoelastic properties of materials by exploring the sound propagation in the material. Different mechanisms can contribute to the sound absorption like viscous effects, thermal conduction and chemical effects. In particular, in liquid systems viscous or viscoelastic effects are the main cause of the sound absorption [13]. Complex modulus of elasticity is an important instrument for viscoelastic characterization of materials [14, 15].

Developing a mathematical relation between sound attenuation and the viscoelastic parameters of the material is of the essence for acoustical characterization of the viscoelasticity. One of the approaches for obtaining these relations is to solve equation of continuity and motion with appropriate initial and boundary conditions, and determining the attenuation as a function of viscoelastic properties of the material.

One of the work done by this order belongs to Assia et al. [16]. The group solved the wave equation for acoustic pressure for Newtonian systems by Laplace transformation method. Hence, the influence of frequency variation, penetration length and relaxation time on the decrease in the sound pressure amplitude is determined by their model.

However, mathematical modeling of sound propagation in viscoelastic media entails to overcome many complications [17]. Hence, using such techniques requires complex mathematics and it is very difficult to deal with set of non-linear equations especially when the thermal effects are considered. Another approach frequently used for getting the attenuation and sound speed as a function of sound frequency and material properties is to propose a solution for the wave equation. Inserting the proposed solution into the governing differential equations, acoustic parameters in terms of these properties are

obtained. These types of approaches are more practical to use than the integral transformation techniques in wave propagation studies [17]. By using this pattern, Sotolongo et al modeled the propagation of small amplitude waves in viscoelastic media [18]. The model shows that two fundamental arguments are strictly dependent on the acoustic parameters; bulk modulus and viscoelasticity of the solution. It is also realized that at low frequencies the polymer solution behaves like a compressible viscous fluid. In this range the impact of increasing polymer concentration is to increase the solution viscosity. At high sound frequencies, the addition of polymer does not influence the behavior of the solution. It is the solvent viscosity that determines the sound propagation. At the intermediate frequencies both longitudinal modulus and solvent viscosity determine the sound propagation. An extensive study on the sound propagation in viscoelastic media including the heat effects by using similar procedure was done by Perepechko et al. [8]. They found that at low frequencies sound propagates adiabatically. However, as frequency gets higher, the sound propagation deviates from adiabatic condition and dissipation of sound energy becomes more observable. In addition, dynamic modulus of elasticity and sound speed increases with frequency, as well.

Aforementioned studies principally dealt with the outcome of the base frequency of sound on propagation. Hence, the propagation of continuous sound wave has been clearly investigated by the former researches. Nevertheless, the sound propagation with discrete ultrasound signal pattern or the effects of pulse repetition frequency have not been apparently explored yet. Therefore, in this study, a mathematical model simulating the discrete sound propagation is developed for the characterization of viscoelastic liquids mainly based on the pulse reputation frequency of ultrasound. It should be noted that base or natural frequency of ultrasound can vary between kHz to MHz ranges. On the other hand, the pulse repetition frequency is in the order of Hz ranges. Therefore, it is possible to probe viscoelastic material properties

or characteristic times of relaxation in the time scales from milliseconds to seconds as opposed to the previous studies. The verification of the proposed mathematical model is performed by comparing its predictions with those of experimental observations obtained during this work.

CHAPTER 2

NON NEWTONIAN FLUID BEHAVIOR AND FLUID VISCOELASTICITY

2.1 Non Newtonian Fluid Behavior

All gases and liquids consisting of small molecules are Newtonian fluids [24]. For them, the ratio of shear stress to shear rate is constant and equal to viscosity. On the other hand, in Non-Newtonian ones, viscosity of the fluids changes with shear rate. Indeed, for some fluids, viscosities change up to 1000 times with shear rate [25]. Non-Newtonian fluids are usually structurally complex fluids such as polymer melts and solutions, lubricants, suspensions and emulsions [24]. Another major difference between Newtonian and Non-Newtonian fluids is the normal stress effects (σ_{xx} , σ_{yy} , σ_{zz}) . In Newtonian fluids, normal stresses are zero; nevertheless, for Non-Newtonian fluids they are non-zero and different.

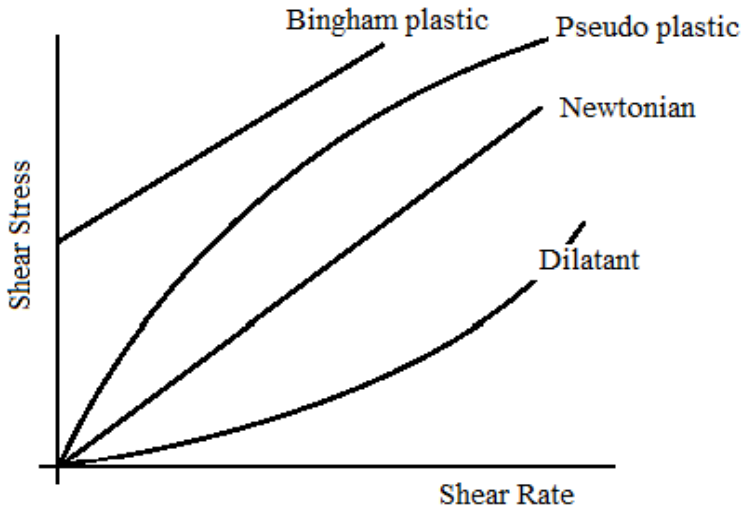

Figure 2.1 Shear stress versus shear rate for various types of fluids

Non-Newtonian fluids can be classified into several types as shown in Figure 2.1. For Pseudo plastic fluids resistance to flow decreases with increasing shear rate, hence they exhibit shear thinning behavior. Most of the polymer melts and solutions are examples to Pseudo plastic fluids. However, in the dilatant fluids, the resistances to flow increase with the shear rate, so they are shears thickening fluids, e.g. some slurries. In addition, in Bingham plastics, like sewage sludge, fluid does not flow until a threshold yield stress. After this stress it flows [15, 26].

However, none of the fluids in Figure 2.1 exhibit time dependent viscoelasticity. Duration of the shear is important for time dependent fluids. For some fluids, under constant shear rate viscosity decreases with time. These types of fluids are called as thixotropic fluids such as paints. For rheopectic fluids like some petroleum products on the other hand, viscosity increases with constant shear rate over a period of time as depicted in Figure 2.2.

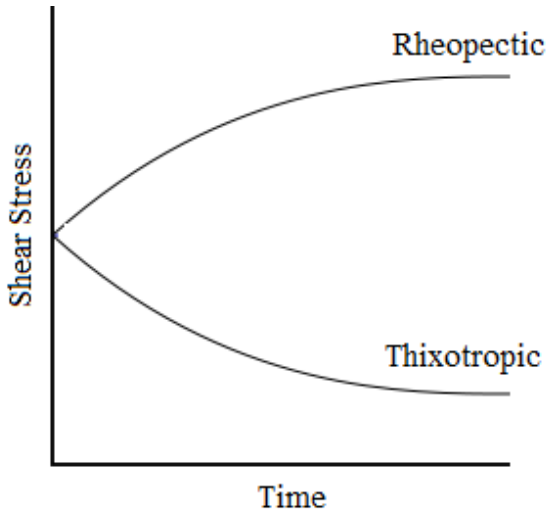

Figure 2.2 Time dependent fluid behavior

2.2 Polymer Melts and Solutions

If the flow characteristics of the polymer melts and solutions are analyzed in a wide range of shear rates, logarithmic curves are obtained (Figure 2.3). Usually it is observed that at lower shear rates, the flow is in the region of "lower Newtonian" with a zero-shear viscosity, η_0. This is due that at lower shear rates intermolecular forces in the polymer chain segments overcome molecular alignment in shear field. Thus, molecules are in entangled state which results in highest resistance to flow. Increasing the shear rate to intermediate region, molecules starts to untangle and flow resistance starts to decrease. At this region the material behaves as a pseudo plastic fluid. Ultimately, after sufficiently high shear rates, molecules are completely aligned hence, resistance to flow is minimized. Here, viscosity reaches to η_∞, which is in the upper "upper Newtonian" region.

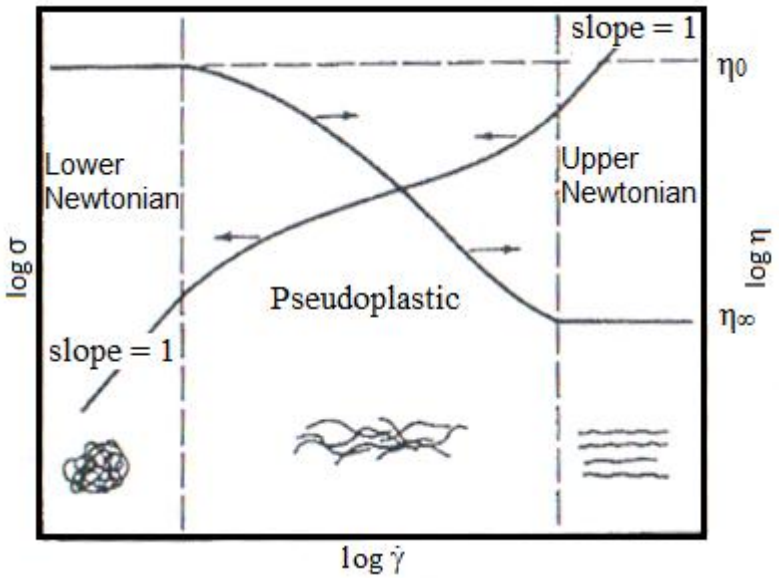

Figure 2.3 Generalized flow properties of polymer melts and solutions [15]

2.3 Fluid Viscoelasticity

Elasticity is the capability of materials to store mechanical energy with no energy dissipation. On the other hand, Newtonian fluid dissipates energy without storing it [17]. Viscoelastic behavior is the combination of both viscous and elastic properties of the materials [28, 30]. One of the most interesting properties of polymers is their viscoelastic behavior when a stress induced to them [31]. For them, stress is a function of both strain (γ_{yx}) and rate of strain ($\dot{\gamma}_{yx}$) [25] .

It should be noted that most of the liquids are not pure Newtonian liquids such that they have not any elastic property. Furthermore, there is not an ideal solid that completely obey Hooke's law at any deformation condition. It is the Maxwell J. who was one of the first people paying attention to this phenomenon [29].

There are two fundamental instruments for the determination of mechanical properties of polymers; stress and strain. When a differential volume in a polymer is considered, the force applied on the faces of this volume is stress

tensor. Strain tensor is the change in the dimensions of the volume under the action of stress tensor.

Stress relaxation is one of the properties of the polymer characterizing time dependent behavior of the polymers. Suppose that suddenly a constant strain γ_0 is applied on a viscoelastic material. Then, one will observe that the stress necessary to sustain this constant strain is a decreasing function of time [25]. This behavior is defined by the relaxation modulus;

$$G(t) = \frac{\sigma_{yx}}{\gamma_0} \tag{2.1}$$

In addition, the initial relaxation modulus is denoted as G_0 (as time goes to 0) and the equilibrium relaxation modulus is shown as G_∞ (as time goes to ∞) .

Viscoelastic properties of polymers can also be investigated by creep test. In creep test, suddenly a constant stress (σ_0) is applied on the material. Meanwhile, the strain is continuously increased to keep stress constant. This is defined by the creep compliance, J [25];

$$J(t) = \frac{\gamma_{yx}(t)}{\sigma_0} \tag{2.2}$$

In addition, creep recovery is another test for investigating viscoelastic properties of polymers. This is done by suddenly removing stress from the material. Then, stress starts to go back to zero.

There are some mathematical models developed to express stress relaxation and creep behaviors of the viscoelastic materials. These models can be schematically represented by spring for denoting elastic behavior and dashpot for denoting viscous behavior. Each model consists of combination of these elements connected to each other serial or parallel. The contribution of elasticity to the viscoelastic properties of material is given by Hooke's Law.

The viscous contribution is expressed by the Newton's Law of viscosity. Some commonly used viscoelastic models are given below.

2.4 Viscoelastic Models

2.4.1 Maxwell Model

Maxwell model is one of the simplest viscoelastic constitutive models. It consists of serially connected spring and dashpot elements [15], as shown in figure 2.4.

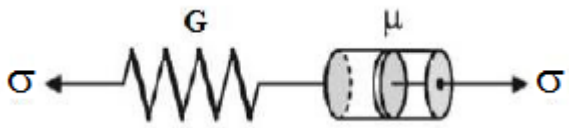

Figure 2.4 Spring-dashpot representation of Maxwell Model

In this model, the spring and dashpot experience the same stress;

$$\sigma = \sigma_{spring} = \sigma_{dashpot} \tag{2.3}$$

In addition, the total strain comes from the summation of the strains of the spring and dashpot;

$$\gamma = \gamma_{spring} + \gamma_{dashpot} \tag{2.4}$$

Taking the derivative with respect to time,

$$\dot{\gamma} = \dot{\gamma}_{spring} + \dot{\gamma}_{dashpot} \tag{2.5}$$

Note that, $\dot{\gamma}_{dashpot} = \sigma_{yx} / \mu$ and $\dot{\gamma}_{spring} = \dot{\sigma}_{yx} / G$, inserting them in to Equation 2.5 gives the Maxwell model as,

$$\sigma_{yx} + \frac{\mu}{G}\frac{\partial \sigma_{yx}}{\partial t} = -\mu \dot{\gamma}_{yx} \tag{2.6}$$

Furthermore, the ratio μ / G in Equation 2.6 is stress relaxation time and can be denoted by τ_0 and changing μ with η_0, the Equation 2.6 will become;

$$\sigma_{yx} + \tau_0 \frac{\partial \sigma_{yx}}{\partial t} = -\eta_0 \dot{\gamma}_{yx} \tag{2.7}$$

Maxwell Model has also two more equivalent forms [15]:

$$\sigma_{yx}(t) = -\int_{-\infty}^{t} \left\{ \frac{\eta_0}{\tau_0} e^{-(t-t')/\tau_0} \right\} \dot{\gamma}_{yx}(t')dt' \tag{2.8}$$

$$\sigma_{yx}(t) = +\int_{-\infty}^{t} \left\{ \frac{\eta_0}{\tau_0^{\,2}} e^{-(t-t')/\tau_0} \right\} \dot{\gamma}_{yx}(t')dt' \tag{2.9}$$

These equations indicate that stress at the time, t depend on the rate of strain at time t and also the rate of strain at all the past times, t'. The term in bracket in Equation 2.8 is also called as relaxation modulus, $G(t - t')$.

To see the creep behavior, differential Equation 2.7 can be solved with constant shear stress, σ_0. Then, it is obtained that,

$$\gamma_{yx}(t) = \gamma_0 + \frac{\sigma_0 t}{\eta_0} = \sigma_0 \left(\frac{1}{G} + \frac{t}{\eta_0}\right) = \eta_0 J(t) \tag{2.10}$$

To see the stress relaxation behavior, differential Equation 2.7 can be solved with constant strain, γ_0. Hence, Equation 2.3 becomes,

$$\sigma_{yx}(t) = \sigma_0 e^{-t/\tau} = \gamma_0 G e^{-t/\tau} = \gamma_0 G(t) \tag{2.11}$$

2.4.2 Voigt-Kelvin Model

In this model, spring and dashpot are assumed to be connected in parallel (Figure2.5). Hence, the strain assisting the dashpot and the spring are same [15],

$$\gamma = \gamma_{spring} = \gamma_{dashpot} \tag{2.12}$$

So, the total stress on the system is the summation of the stress on the spring and the dashpot.

$$\sigma = \sigma_{spring} + \sigma_{dashpot} \tag{2.13}$$

Combining Equation 2.12 and Equation 2.13 gives the governing differential equation for Voigt-Kelvin model.

$$\sigma_{yx} = \eta_0 \frac{\partial \gamma_{yx}}{\partial t} + G\gamma_{yx} \tag{2.14}$$

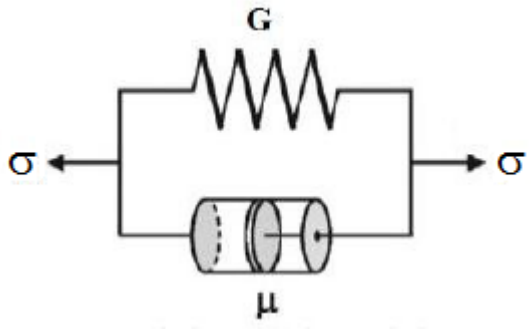

Figure 2.5 Spring-dashpot representation of Voigt-Kelvin Model

Creep test can be done by solving differential Equation 2.14 with constant shear stress, σ_0. Then, it is obtained that [15],

$$\gamma_{yx}(t) = \frac{\sigma_0}{G}(1 - e^{-t/\tau}) = \sigma_0 J(t) \tag{2.15}$$

If the stress is removed when the equilibrium is reached, the strain becomes,

$$\gamma_{yx}(t) = \frac{\sigma_0}{G} e^{-t/\tau} \tag{2.16}$$

2.4.3 Generalized Maxwell Model

The generalized Maxwell model considers n Maxwell elements connected parallel to each other [15] as shown in Figure 2.6.

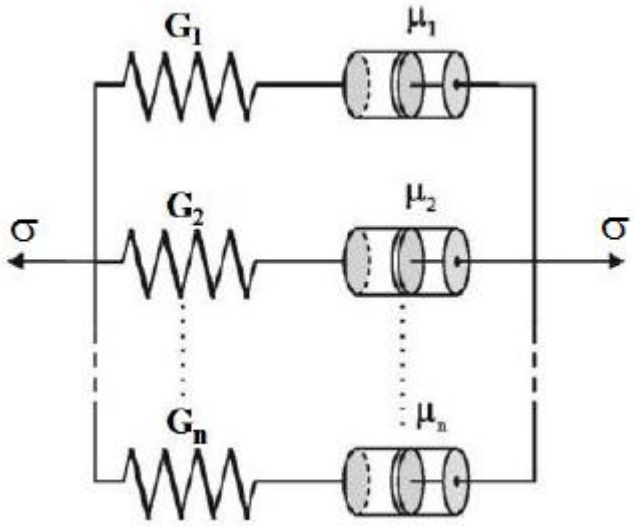

Figure 2.6 Spring-dashpot representation of Generalized Maxwell Model

Now, the stress for each Maxwell element is given by,

$$\sigma_{yx,i}(t) = \gamma_0 G_i e^{-t/\tau_i} \tag{2.17}$$

A constant strain, γ_0 is applied to all the Maxwell elements, and then using the superposition principle summation of stresses by each element is calculated as,

$$\sigma_{yx}(t) = \sum_{i=1}^{n} \sigma_{yx,i}(t) = \gamma_0 \sum_{i=1}^{n} G_i e^{-t/\tau_i} \tag{2.18}$$

where

$$\tau_i = \eta_i / G_i \tag{2.19}$$

Equation 2.18 can also be represented as [15],

$$\sigma_{yx}(t) = -\int_{-\infty}^{t} \left\{ \sum_{i=1}^{n} \frac{\eta_{0,i}}{\tau_{0,i}} e^{-(t-t')/\tau_{0,i}} \right\} \dot{\gamma}_{yx}(t')dt' \tag{2.20}$$

This equation can also represented in terms of relaxation modulus,

$$\sigma_{yx}(t) = -\int_{-\infty}^{t} G(t-t')\dot{\gamma}_{yx}(t')dt' \tag{2.21}$$

2.4.4 Generalized Voigt-Kelvin Model

The generalized Voigt-Kelvin model considers n Voigt-Kelvin elements connected in series to each other [15] as shown in Figure 2.7.

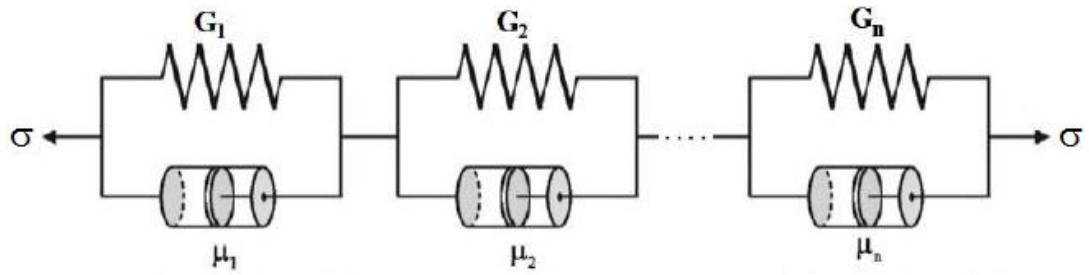

Figure 2.7 Spring-dashpot representation of Generalized Voigt-Kelvin Model

Now, the strain for each Voigt-Kelvin element is given by,

$$\gamma_{yx}(t) = \frac{\sigma_0}{G}(1-e^{-t/\tau}) = \sigma_0 J(t) \tag{2.15}$$

A constant strain, σ_0 is applied to all the Voigt-Kelvin elements, and then using the superposition principle summation of strains by each element is calculated as,

$$\gamma_{yx}(t) = \sum_{i=1}^{n} \frac{\sigma_0}{G_i}(1-e^{-t/\tau_i}) \tag{2.22}$$

2.4.5 Relaxation Spectra

Summation of Maxwell elements gives the distribution of relaxation times "τ_n" with respect to corresponding modulus "G_n". When the number of relaxation times is increased infinitely, G (t) takes the integral form of,

$$G(t) = \int_0^{\infty} G_k(\tau) e^{-t/\tau} d\tau \tag{2.23}$$

Here, $G_k(\tau)$ is the relaxation spectrum.

2.5 Relation between Stress and Strain

The relation between stress and strain can be represented by,

$$\sigma = E^* \gamma \tag{2.24}$$

Here, E^* represents the complex modulus of elasticity. The real part of E^* gives dynamic modulus of elasticity while the imaginary part of E^* gives the loss modulus. In other words,

$$E^*(w) = E'(w) + E''(w) \tag{2.25}$$

The dynamic modulus of elasticity characterizes the amount of energy stored while the loss modulus is related to the energy dissipation characteristics of a material.

Suppose that a sinusoidal stress is being applied on the material such that,

$$\sigma = \sigma_0 \sin(wt) \tag{2.26}$$

If the material exhibits linear viscoelastic behavior, the strain will also change sinusoidally with a phase shift,

$$\varepsilon = \varepsilon_0 \sin(wt - \delta) \tag{2.27}$$

where

δ is the phase shift.

It should also be noted that the value of E' increases or remains constant with increase in the frequency.

The absolute value of complex modulus of elasticity can be found by,

$$\left|E(w)^*\right| = \sqrt{(E(w)')^2 + (E(w)'')^2} = \frac{\sigma_0}{\gamma_0} \tag{2.28}$$

The phase shift δ gives the slope of mechanical losses or loss tangent, namely,

$$\tan\delta = \frac{E''}{E'} \tag{2.29}$$

The relation between the components of E^* and phase shift, δ can be constructed by,

$$E' = \left|E^*\right|\cos\delta \tag{2.30}$$

$$E'' = \left|E^*\right|\sin\delta \tag{2.31}$$

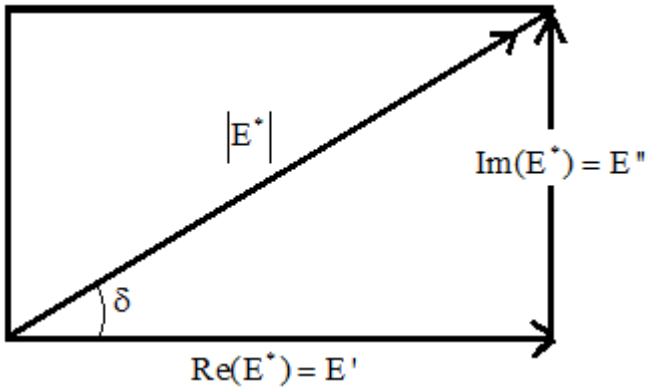

Figure 2.8 the relation between the components of E^* and phase shift δ

The concept of complex compliance can be established by,

$$J^* = \frac{1}{E^*} = J' - iJ'' \tag{2.32}$$

Here, J' is dynamic or storage compliance and J'' is the loss compliance. Since the relation between E^* and J^* is known, J^* and its components can readily be written in terms of E^*, E' and E'',

$$J^* = \frac{\frac{1}{E'} - i\frac{1}{E'}\tan\delta}{1+\tan^2\delta} \tag{2.33}$$

and

$$J' = \frac{\frac{1}{E'}}{1+\tan^2\delta} \tag{2.34}$$

$$J'' = \frac{\frac{\tan\delta}{E'}}{1+\tan^2\delta} = \frac{\frac{1}{E''}}{1+(\tan^2\delta)^{-1}} \tag{2.35}$$

CHAPTER 3

SOUND AND MATERIAL INTERACTIONS

3.1 Nature of Sound

Sound is mechanical vibration and/or mechanical waves, which is an oscillation of pressure transmitted through an elastic media [20]. It is first elaborated by Newton, in his book Principia, as pressure wave propagating through the adjacent particles and his pioneering studies were followed by the works of Euler, Lagrange and d'Alembert [21]. During the 19th century, theoretical background of acoustics was established. "The Theory of Sound" by Rayleigh 1886 is still used as important reference by the researchers.

To handle the physics of sound, sound waves are often mathematically interpreted by differential equations, wave equations. Wave equations are generally are in the form of partial differential equations since the dependent variable, usually sound pressure or displacement, is a function of both position and time [21]. Propagating sinusoidally, sound has a frequency and the frequencies above 20 kHz correspond to ultrasound [21]. Sound can propagate through the media in two different fashion; longitudinal and transverse wave propagation [22] . In longitudinal wave propagation, the displacements of the particles are parallel to the direction of the propagation of the wave (Figure 3.1). In this type, the region where the sound is passing through is compressed, then it is relaxed, ultimately particles come back to their equilibrium position [19]. In the case of transverse propagation, on the other hand, the displacements of the particles are perpendicular to the direction of the sound

propagation (Figure 3.1). Transverse waves can propagate in solids; nevertheless, fluids are not able to sustain transverse wave as there is no mechanism in liquids and gases for driving motion perpendicular to the propagation of wave [22].

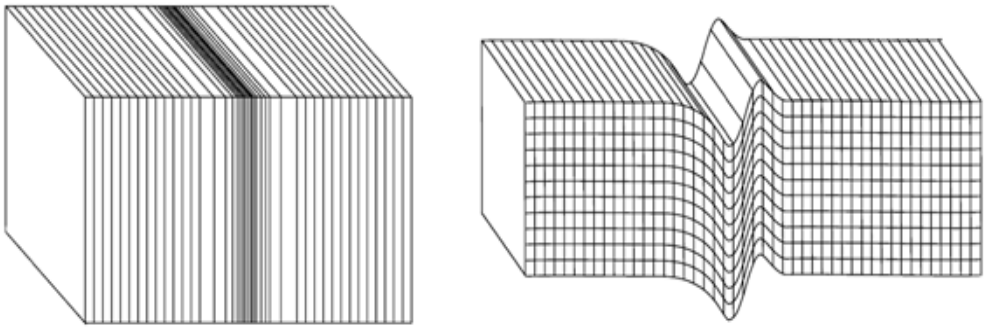

Figure 3.1 Schematic representation of longitudinal (left) and transverse (right) wave propagation [23]

3.1.1 Sound Attenuation

Sound attenuation is the measure of the decrease in the sound amplitude or level or the energy dissipated to heat through the viscous effects of the material [23]. The energy loss stems from the scattering, reflection and absorption of the sound signal. The level of the sound attenuation is determined by both the frequency of ultrasound and the material properties. It can be calculated from;

$$\alpha = \frac{1}{x_2 - x_1} \ln\left(\frac{A_1}{A_2}\right) \tag{3.1}$$

where α, x and A refer to the sound attenuation, coordinates and the sound amplitude, respectively. Subscripts are used to mark the positions.

3.2 Relation between Complex Modulus and Acoustic Parameters

Physical and chemical natures of a material have a strong influence on the sound attenuation and sound propagation speed [8]. For example, the relation between the complex modulus of elasticity and these aspects are given through the following equations;

$$M' = \frac{\rho c^2 \left[1 - \left(\frac{\alpha\lambda}{2\pi} \right)^2 \right]}{\left[1 + \left(\frac{\alpha\lambda}{2\pi} \right)^2 \right]^2} \tag{3.2}$$

$$M'' = \frac{2\rho c^2 \frac{\alpha\lambda}{2\pi}}{\left[1 + \left(\frac{\alpha\lambda}{2\pi} \right)^2 \right]^2} \tag{3.3}$$

where M' and M'' are the storage and loss components. Then the complex modulus of elasticity, M^*, is given by the following equation;

$$M^* = M' + iM'' \tag{3.4}$$

Derivation of Equations 3.2 and 3.3 are given in Appendix A.1. Bonding energy between the atoms forming the main chain of the polymer and the intermolecular forces between the neighboring polymer chains determines the change in the complex modulus of elasticity as a function of frequency. In the acoustic experiments, each one of these forces can reveal itself. To illustrate, the sound propagation speed in a polymer fiber in the direction of the fibers orientation is about $(8-12)x10^5 cm/s$. Bonding energy between atoms plays dominant role for this speed. However, when it is measured not on the direction of orientation, intermolecular forces determines the velocity and it is detected about $(1.2-1.5)x10^5 cm/s$ [34, 35].

The dynamic modulus of elasticity provides many indications about the physical situation of a polymer. For example, intermolecular forces are greater

in glassy state of polymers than the rubbery state. Hence, the values of dynamic modulus of elasticity in the glassy polymers are in the order of $10^{10}\,\mathrm{dyn/cm^2}$, while it is in the order of $(10^6 - 10^7)$ dyn/cm^2 in the rubbery polymers. Any change in the intermolecular structure of polymers also alters the dynamic modulus of elasticity, so that sound propagation is also affected.

As a result, sound speed and amplitude attenuation provide information about the mechanical properties, physical and chemical structure and the composition of the material. Besides, these parameters can also be used for the determination of the relaxation times of the materials.

3.3 Physical Interpretation of Sound Absorption

The relaxation theory clarifies the fundamental acoustic properties of polymers. Under the action of wave propagation, the system deviates from the thermodynamic equilibrium state. When the wave propagation is interrupted the system assumes back its thermodynamic equilibrium state by internal forces. This period is called as relaxation time, i.e. the time necessary for reaching equilibrium is the relaxation time. Various kinds of molecular motions have contribution on the system to come back thermodynamic equilibrium from the transition state. A proper relaxation process is defined by matching relaxation times to corresponding molecular motion. It is necessary to adjust the experimental duration with the relaxation time in the same order of magnitude to determine the relaxation process with corresponding molecular motion [8].

3.4 Material Characterization by Acoustic Methods

Ultrasonic techniques for the investigation of polymers are based on pulsed ultrasound and operate in two modes; pulse-echo and transmittance mode. In pulse-echo mode (Figure 3.2), first, ultrasonic wave (A_0) is emitted by a transducer. Then, some part of it (A_{0r}) is reflected between the interface of the

transducer and the material. This gives the first echo. Meanwhile, the remaining part of the wave (A_{1r}) propagates through the material. When it reaches to the interface between the material and its bordering, some part of it (A_{0r}) is reflected. This gives the second echo. Hence, the sound speed and attenuation can be determined by measuring the time between two successive echoes and their amplitudes.

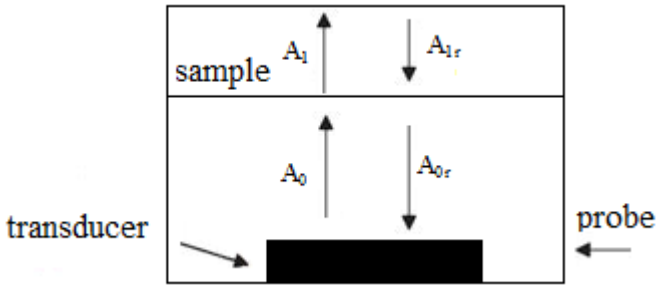

Figure 3.2 Representation of pulse-echo mode [23]

In the transmission method (Figure 3.3), two probes are necessary, one is used as transmitter and the other is used as receiver. Sound emitted by the transducer with A_0 amplitude eventually reaches to the receiver as A_2. The sound attenuation here can be determined by comparing the amplitudes of the echo received with and without material of interest between the transducers.

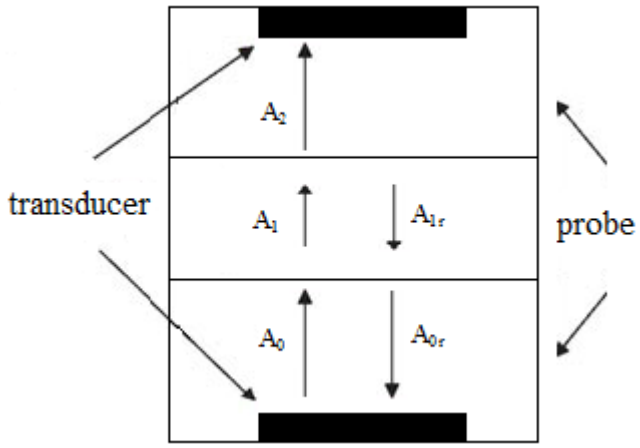

Figure 3.3 Representation of transmission mode [23]

CHAPTER 4

MATHEMATICAL MODELLING OF ULTRASOUND PROPAGATION IN A VISCOELASTIC MATERIAL

4.1 Propagation of Sound Waves in Viscoelastic Medium

In this part, modeling of sound propagating in a viscoelastic media is presented. Specifically, the interaction between successive ultrasound pulses and the material is modeled. Eventually, the model will be instrumental to probe viscoelastic properties of the material through the modulated ultrasound pulses.

The model begins with the displacement of the particles in the medium when subjected to continuous wave propagation.

$$u = u_{0k} e^{iwt - \sigma x} \tag{4.1}$$

where σ is complex wave number;

$$\sigma = \alpha + i\frac{w}{c} \tag{4.2}$$

However, Equation 4.1 should be modified to capture the propagation of modulated waves in a medium. In Figure 4.1, discrete or modulated wave propagation is schematically represented. Here, discrete signals are sent successively, and pulse length of each signal is denoted as “n”. In addition, duration between the end of a pulse and the start of its successor (PRF) is denoted as “a”.

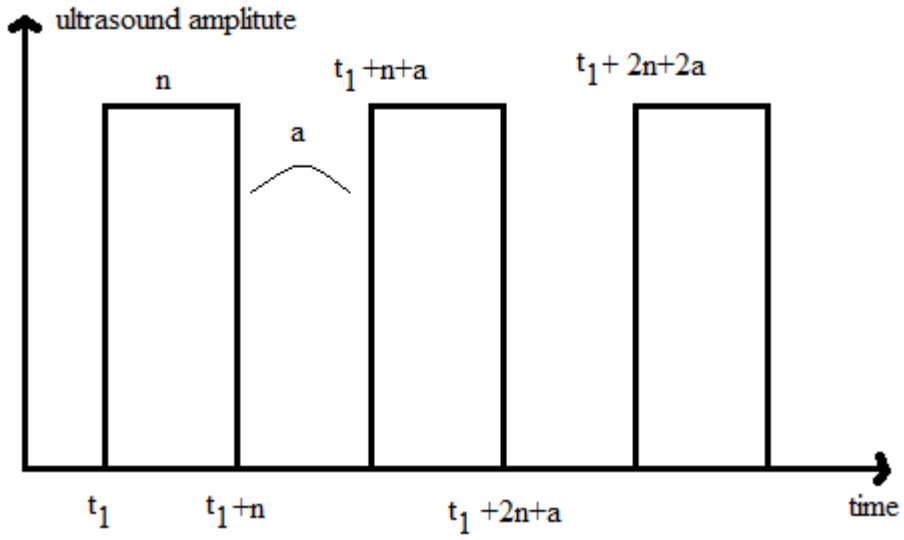

Figure 4.1 Representation of discrete sound waves in the medium

At time, t_1 the first sound signal is sent to sample. Therefore, between the time t_1 and t_1+n, Equation 4.1 models the displacement of the particles. After the time, t_1+n, the sound is no longer sent to the medium. Hence, to start and stop the wave mathematically at the time, t_1 and t_1+n, respectively, the following equation can be written;

$$u = H(t - t_1)u_{0k}e^{iwt-\sigma x} - H(t - (t_1 + n))u_{0k}e^{iwt-\sigma x} \qquad (4.3)$$

where H is the Heaviside unit step function, namely;

$$H(t-a) = \begin{Bmatrix} 1 & \text{if} & t > a \\ 1/2 & \text{if} & t = a \\ 0 & \text{if} & t < a \end{Bmatrix}$$

The first term in Equation 4.3 is equal to $u_{0k}e^{iwt-\sigma x}$ after the time, t_1; however, the second term is still zero until the time, t_1+n. After time, t_1+n the second term is converted to $-u_{0k}e^{iwt-\sigma x}$; hence, these terms vanish each other, and Equation 4.3 becomes zero. However, this is not enough to model the system. This can only model the system between time t_1 and t_1+n. After the time t_1+n, the particles are not in their equilibrium positions, but the particles starts to

settle their equilibrium positions. Therefore, a recovery term should be included in the model equation for the particles' recovery to their equilibrium positions. This can be expressed by adding a recovery function to Equation 4.3. At time, t_1+n the displacement is $u_{0k}e^{iw(t_1+n)-\sigma x}$, constituting the initial condition of the recovery term, which can be obtained by the use of viscoelastic constitutive equations. Figure 4.2 is an illustrative figure representing the behavior of the medium or the output when exposed to the discrete sound wave propagation or the input.

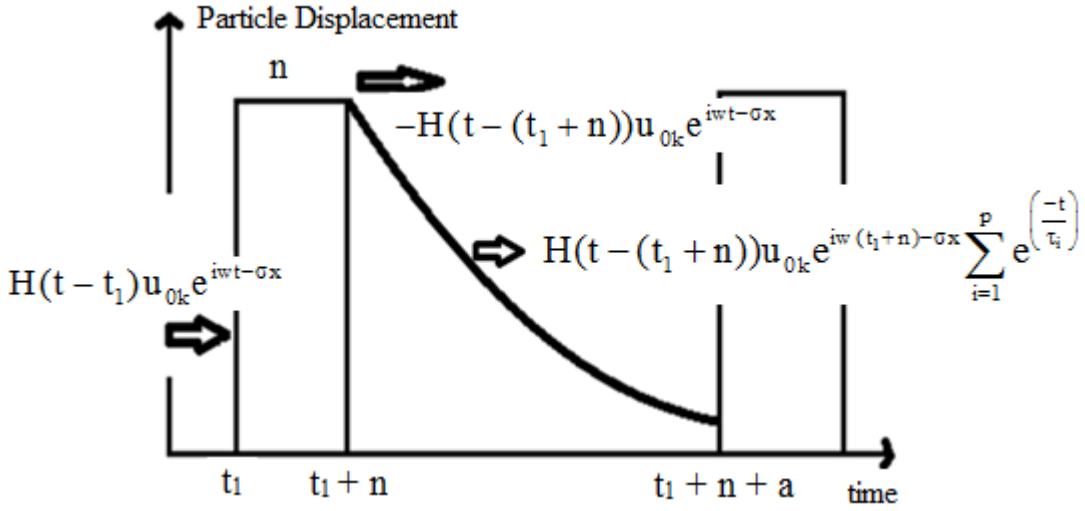

Figure 4.2 Representation of the displacement of particles with time

For the recovery of molecules generalized Voigt-Kelvin model is used. This is one of the simplest models to explain the behavior of the molecules under action of constant loading and their recovery when the stress is removed. The Voigt-Kelvin analogy fits the case in discrete wave propagation in viscoelastic media. Since, during the wave propagation at a fixed position, the molecules are first under the action of the pressure of the ultrasound. Although the wave has a sinusoidal character, the mean amplitude of the wave pressure remains constant. Hence, in this period the molecules at this position can be accepted to be exposed to a constant loading. When the wave stops, the molecules tend to recover their equilibrium position. Hence, this behavior can be added to

model by inserting the recovery of molecules according to Voigt-Kelvin model. Thus, when the stress is removed, they will come back to equilibrium position according to Voigt-Kelvin by;

$$u = u_i \sum_{i=1}^{p} e^{\left(\frac{-t}{\tau_i}\right)} \tag{4.4}$$

By adding this term into Equation 4.3, and making the similar calculation for the second wave, it is obtained that;

$$\begin{aligned} u &= H(t-t_1)u_{0k}e^{iwt-\sigma x} - H(t-(t_1+n))u_{0k}e^{iwt-\sigma x} \\ &+H(t-(t_1+n))u_{0k}e^{iw(t_1+n)-\sigma x}\sum_{i=1}^{p} e^{\left(\frac{-t}{\tau_i}\right)} \\ &+H(t-(t_1+n+a))u_{0k}e^{iwt-\sigma x} - H(t-(t_1+2n+a))u_{0k}e^{iwt-\sigma x} \\ &+H(t-(t_1+2n+a))u_{0k}e^{iw(t_1+2n+a)-\sigma x}\sum_{i=1}^{p} e^{\left(\frac{-(t-(t_1+2n+a))}{\tau_i}\right)} \end{aligned} \tag{4.5}$$

Equation 4.5 can be generalized for "m" number waves as,

$$\begin{aligned} u = \sum_{j=0}^{m} u_{0k}e^{-\sigma x}[&e^{iwt}H(t-(t_1+j(n+a))) - e^{iwt}H(t-(t_1+(j+1)n+ja)) \\ &+e^{iw(t_1+(j+1)n+ja)}H(t-(t_1+(j+1)n+ja))\sum_{n=1}^{p} e^{\left(\frac{-(t-(t_1+(j+1)n+ja))}{\tau_i}\right)}] \end{aligned} \tag{4.6}$$

Temperature and density variations can also be expressed similar to the displacement;

$$\begin{aligned} T = \sum_{j=0}^{m} T_{0k}e^{-\sigma x}[&e^{iwt}H(t-(t_1+j(n+a))) - e^{iwt}H(t-(t_1+(j+1)n+ja)) \\ &+e^{iw(t_1+(j+1)n+ja)}H(t-(t_1+(j+1)n+ja))\sum_{n=1}^{p} e^{\frac{-(t-(t_1+(j+1)n+ja))}{\tau_i}}] \end{aligned} \tag{4.7}$$

$$\rho = \sum_{j=0}^{m} \rho_{0k} e^{-\sigma x} [e^{iwt} H(t-(t_1+j(n+a))) - e^{iwt} H(t-(t_1+(j+1)n+ja)) + e^{iw(t_1+(j+1)n+ja)} H(t-(t_1+(j+1)n+ja)) \sum_{n=1}^{p} e^{\frac{-(t-(t_1+(j+1)n+ja))}{\tau_i}}] \quad (4.8)$$

Furthermore, the pressure variation can also be defined as;

$$P = \sum_{j=0}^{m} P_{0k} e^{-\sigma x} [e^{iwt} H(t-(t_1+j(n+a))) - e^{iwt} H(t-(t_1+(j+1)n+ja)) + e^{iw(t_1+(j+1)n+ja)} H(t-(t_1+(j+1)n+ja)) \sum_{n=1}^{p} e^{\frac{-(t-(t_1+(j+1)n+ja))}{\tau_i}}] \quad (4.9)$$

Now, proposed solutions for u, ρ and T are obtained. Here, the main quantity characterizing the u, ρ and T variations is "σ". Hence, in order to identify the u, ρ and T variations through "σ", these suggested solutions for u, ρ and T, should be inserted into the governing differential equations. Dependent variables in the governing differential equations should be written in terms of u, ρ and T. Hence, some simplifications and modifications are done in the equation of continuity, motion and energy. Their derivations are shown in Appendix A.2. Ultimately, the governing differential equations take the form of;

$$\frac{\partial \rho}{\partial t} + \rho_0 \frac{\partial^2 u}{\partial x \partial t} = 0 \quad (4.10)$$

$$\rho_0 \frac{\partial^2 u}{\partial t^2} + K_T \alpha_V \frac{\partial T}{\partial x} - L \frac{\partial^2 u}{\partial x^2} = 0 \quad (4.11)$$

$$C_V \frac{\partial T}{\partial t} - \frac{T \alpha_V K_T}{\rho_0^2} \frac{\partial \rho}{\partial t} - \frac{k}{\rho_0} \frac{\partial^2 T}{\partial x^2} = 0 \quad (4.12)$$

To make simplification in the u, ρ and T, lets define A and B as,

$$A = H(t-(t_1+j(n+a))) - H(t-(t_1+(j+1)n+ja)) \tag{4.13}$$

$$B = e^{iw(t_1+(j+1)n+ja)} H(t-(t_1+(j+1)n+ja)) \tag{4.14}$$

Substituting the density, displacement and temperature into our governing differential equations, equation of continuity becomes,

$$\sum_{j=0}^{m}\left[\rho_{0k}e^{-\sigma x}\left(Ae^{iwt}iw + B\sum_{i=1}^{p}\left(\frac{-1}{\tau_i}\right)e^{\left(\frac{-(t-(t_1+(j+1)n+ja))}{\tau_i}\right)}\right)\right]$$
$$+\rho_0\sum_{j=0}^{m}\left[u_{0k}e^{-\sigma x}(-\sigma)\left(Ae^{iwt}iw + B\sum_{i=1}^{p}\left(\frac{-1}{\tau_i}\right)e^{\left(\frac{-(t-(t_1+(j+1)n+ja))}{\tau_i}\right)}\right)\right] = 0 \tag{4.15}$$

Similarly equation of motion becomes,

$$\rho_0\sum_{j=0}^{m}\left[u_{0k}e^{-\sigma x}\left(-Ae^{iwt}w^2 + B\sum_{i=1}^{p}\left(\frac{-1}{\tau_i}\right)^2 e^{\left(\frac{-(t-(t_1+(j+1)n+ja))}{\tau_i}\right)}\right)\right]$$
$$+K_T\alpha_V\sum_{j=0}^{m}\left[T_{0k}e^{-\sigma x}(-\sigma)\left(Ae^{iwt} + B\sum_{i=1}^{p}e^{\left(\frac{-(t-(t_1+(j+1)n+ja))}{\tau_i}\right)}\right)\right]$$
$$-L\sum_{j=0}^{m}\left[u_{0k}e^{-\sigma x}(-\sigma)^2\left(Ae^{iwt} + B\sum_{i=1}^{p}e^{\left(\frac{-(t-(t_1+(j+1)n+ja))}{\tau_i}\right)}\right)\right] = 0 \tag{4.16}$$

Finally, equation of energy becomes as,

$$C_V \sum_{j=0}^{m}\left[T_{0k} e^{-\sigma x}\left(Ae^{iwt} iw + B\sum_{i=1}^{p}\left(\frac{-1}{\tau_i}\right) e^{\left(\frac{-(t-(t_1+(j+1)n+ja))}{\tau_i}\right)}\right)\right]$$

$$-\frac{T\alpha_V K_T}{\rho_0^{\,2}} \sum_{j=0}^{m}\left[\rho_{0k} e^{-\sigma x}\left(Ae^{iwt} iw + B\sum_{i=1}^{p}\left(\frac{-1}{\tau_i}\right) e^{\left(\frac{-(t-(t_1+(j+1)n+ja))}{\tau_i}\right)}\right)\right]$$

$$-\frac{k}{\rho_0} \sum_{j=0}^{m}\left[T_{0k} e^{-\sigma x}(-\sigma)^2\left(Ae^{iwt} + B\sum_{i=1}^{p} e^{\left(\frac{-(t-(t_1+(j+1)n+ja))}{\tau_i}\right)}\right)\right] = 0 \qquad (4.17)$$

For further simplification let's define N, M and S as,

$$N = B\sum_{i=1}^{p}\left(\frac{-1}{\tau_i}\right) e^{\left(\frac{-(t-(t_1+(j+1)n+ja))}{\tau_i}\right)} \qquad (4.18)$$

$$M = B\sum_{i=1}^{p}\left(\frac{-1}{\tau_i}\right)^2 e^{\left(\frac{-(t-(t_1+(j+1)n+ja))}{\tau_i}\right)} \qquad (4.19)$$

$$S = B\sum_{i=1}^{p} e^{\left(\frac{-(t-(t_1+(j+1)n+ja))}{\tau_i}\right)} \qquad (4.20)$$

Each of the equations has number of solution; however, for non-trivial solution of the set of equations, the determinant of the following matrix should be zero.

$$\det\begin{vmatrix} \rho_{0k} & u_{0k} & T_{0k} \\ \sum_{j=0}^{m}[Ae^{iwt} iw + N] & -\rho_0\sum_{j=0}^{m}[(-\sigma)(Ae^{iwt} iw + N)] & 0 \\ 0 & \rho_0\sum_{j=0}^{m}[-Ae^{iwt} w^2 + M] - L\sum_{j=0}^{m}[(-\sigma)^2(Ae^{iwt} + S)] & K_T\alpha_V\sum_{j=0}^{m}[(-\sigma)(Ae^{iwt} + S)] \\ -\frac{T\alpha_V K_T}{\rho_0^{\,2}}\sum_{j=0}^{m}[Ae^{iwt} iw + N] & 0 & -\frac{k}{\rho_0}\sum_{j=0}^{m}[(-\sigma)^2(Ae^{iwt} + S)] + C_V\sum_{j=0}^{m}[Ae^{iwt} iw + N] \end{vmatrix} = 0$$

(4.21)

Taking the determinant yields,

$$\left(\sum_{j=0}^{m}[Ae^{iwt}iw+N]\right)\left(\rho_0\sum_{j=0}^{m}((-A)e^{iwt}w^2+M)\right)$$
$$\left(-L\sum_{j=0}^{m}[(-\sigma)^2(Ae^{iwt}+S)]\right)\left(-\frac{k}{\rho_0}\sum_{j=0}^{m}[(-\sigma)^2(Ae^{iwt}+S)]+C_V\sum_{j=0}^{m}[Ae^{iwt}iw+N]\right)$$
$$\left(-\rho_0(-\sigma)\sum_{j=0}^{m}[Ae^{iwt}iw+N]\right)\left(K_T\alpha_V(-\sigma)\sum_{j=0}^{m}[Ae^{iwt}iw+S]\right)\left(\frac{T\alpha_V K_T}{\rho_0{}^2}\sum_{j=0}^{m}[Ae^{iwt}iw+N]\right)=0 \quad (4.22)$$

Hence, rearranging we ultimately obtain;

$$\sigma^4\left\{\frac{Lk}{\rho_0}\left(\sum_{j=0}^{m}[Ae^{iwt}+S]\right)\left(\sum_{j=0}^{m}[Ae^{iwt}iw+N]\right)\left(\sum_{j=0}^{m}[Ae^{iwt}+S]\right)\right\}$$
$$+\sigma^2\left\{-k\left(\sum_{j=0}^{m}[(-A)^2e^{iwt}w^2+M]\right)\left(\sum_{j=0}^{m}[Ae^{iwt}iw+N]\right)\left(\sum_{j=0}^{m}[Ae^{iwt}+S]\right)\right.$$
$$-LC_V\left(\sum_{j=0}^{m}[Ae^{iwt}iw+S]\right)\left(\sum_{j=0}^{m}[Ae^{iwt}iw+N]\right)\left(\sum_{j=0}^{m}[Ae^{iwt}iw+N]\right)$$
$$\left.-\frac{T\alpha_V{}^2K_T{}^2}{\rho_0}\left(\sum_{j=0}^{m}[Ae^{iwt}iw+N]\right)\left(\sum_{j=0}^{m}[Ae^{iwt}+S]\right)\left(\sum_{j=0}^{m}[Ae^{iwt}iw+N]\right)\right\}$$
$$\left\{\rho_0C_v\left(\sum_{j=0}^{m}[(-A)e^{iwt}w^2+M]\right)\left(\sum_{j=0}^{m}[Ae^{iwt}iw+N]\right)\left(\sum_{j=0}^{m}[Ae^{iwt}iw+N]\right)\right\}=0 \quad (4.23)$$

This is the dispersion equation relating the viscoelastic properties of the media with the acoustic parameters.

4.2 Further Simplification of the Mathematical Model

As it stands Equation 4.23 is too complicated to be employed. Possible simplifications for practical applications can make it easier to employ the equation. For this purpose, to evaluate Equation 4.23 term by term, now let's define y1, y2, y3, y4 and y5 as;

$$y1 = \left[\frac{Lk}{\rho_0} \left(\sum_{j=0}^{m} [Ae^{iwt} + S] \right) \left(\sum_{j=0}^{m} [Ae^{iwt} iw + N] \right) \left(\sum_{j=0}^{m} [Ae^{iwt} + S] \right) \right] \quad (4.24)$$

$$y2 = \left[-k \left(\sum_{j=0}^{m} [(-A)^2 e^{iwt} w^2 + M] \right) \left(\sum_{j=0}^{m} [Ae^{iwt} iw + N] \right) \left(\sum_{j=0}^{m} [Ae^{iwt} + S] \right) \right] \quad (4.25)$$

$$y3 = \left[-LC_V \left(\sum_{j=0}^{m} [Ae^{iwt} iw + S] \right) \left(\sum_{j=0}^{m} [Ae^{iwt} iw + N] \right) \left(\sum_{j=0}^{m} [Ae^{iwt} iw + N] \right) \right] \quad (4.26)$$

$$y4 = \left[-\frac{T\alpha_V{}^2 K_T{}^2}{\rho_0} \left(\sum_{j=0}^{m} [Ae^{iwt} iw + N] \right) \left(\sum_{j=0}^{m} [Ae^{iwt} + S] \right) \left(\sum_{j=0}^{m} [Ae^{iwt} iw + N] \right) \right] \quad (4.27)$$

$$y5 = \left[\rho_0 C_v \left(\sum_{j=0}^{m} [(-A)e^{iwt} w^2 + M] \right) \left(\sum_{j=0}^{m} [Ae^{iwt} iw + N] \right) \left(\sum_{j=0}^{m} [Ae^{iwt} iw + N] \right) \right] \quad (4.28)$$

so, Equation 4.23 is converted to;

$$\sigma^4 (y1) + \sigma^2 (y2 + y3 + y4) + y5 = 0 \quad (4.29)$$

Although, physical properties of liquids vary, the magnitudes of the properties are usually in the same order. Hence, the magnitude of each term in Equation 4.29 can be evaluated by the approximate properties of a liquid.

The physical properties are taken as k=0.5 W/m K, ρ_0=1000 kg/m^3, C_V=4140 J/kg K, α_v=2.56x10^{-4} K^{-1}, L=K_T=10^9 Pa and T=300 K.

and the average value of the wave number "σ" can be taken as;

$$\sigma \approx 10^4 + 10^3 i$$

Inserting them into Equation 4.29 for m=50;

$$y1 \approx 2.257x10^{9} + i2.513x10^{15}$$
$$\sigma^4 y1 \approx -8.61x10^{27} + i9.3x10^{33}$$

$$y2 \approx 1.189x10^{22} + i3.349x10^{27}$$

$$y3 \approx 6.641x10^{34} + i7.395x10^{40}$$

$$y4 \approx 6.985x10^{28} - i2.481x10^{23}$$

So for the term (y2+y3+y4), y3 is the dominating term among the others. Hence, they can be neglected.

$$\sigma^2(y2 + y3 + y4) \approx -1.985x10^{42} + i1.423x10^{50}$$

In addition, magnitude of the term "$\sigma^4 y1$" is very small with respect to "$\sigma^2(y2 + y3 + y4)$", so it can also be neglected.

$$y5 = 5.226x10^{43} - i1.856x10^{49}$$

Therefore, Equation 4.29, reduces to

$$\sigma^2 y3 + y5 = 0 \tag{4.30}$$

or in open form,

$$\sigma^2 \left\{ -LC_V \left(\sum_{j=0}^{m} [Ae^{iwt} iw + S] \right) \left(\sum_{j=0}^{m} [Ae^{iwt} iw + N] \right) \left(\sum_{j=0}^{m} [Ae^{iwt} iw + N] \right) \right\}$$
$$+\rho_0 C_v \left\{ \left(\sum_{j=0}^{m} [(-A)e^{iwt} w^2 + M] \right) \left(\sum_{j=0}^{m} [Ae^{iwt} iw + N] \right) \left(\sum_{j=0}^{m} [Ae^{iwt} iw + N] \right) \right\} = 0$$

Further simplification gives, (4.31)

$$\sigma^2 = \frac{\rho_0}{L} \frac{\sum_{j=0}^{m}[(-A)e^{iwt}w^2 + M]}{\sum_{j=0}^{m}[Ae^{iwt}iw + S]} \tag{4.32}$$

or

$$\sigma = \sqrt{\frac{\rho_0}{L} \frac{\sum_{j=0}^{m}[(-A)e^{iwt}w^2 + M]}{\sum_{j=0}^{m}[Ae^{iwt}iw + S]}} \tag{4.33}$$

Hence, density and longitudinal modulus is much more dominant for the determination of σ. Heat effects and thermal expansion is negligibly small. Indeed, it will be shown in the results part by the simulations that temperature variation during the wave propagation is too small.

4.3 Spectral Analysis

In this part it is questioned whether changing some acoustic parameters can filter a relaxation time while the others in the spectrum are discarded. If it is possible, by changing the acoustic parameters, corresponding relaxation times can be obtained. Hence, relaxation spectrum is obtained. Coming back to the equation for pressure variation;

$$P = \sum_{j=0}^{m} P_{0k} e^{-\sigma x}[e^{iwt}H(t-(t_1+j(n+a))) - e^{iwt}H(t-(t_1+(j+1)n+ja)) + e^{iw(t_1+(j+1)n+ja)}H(t-(t_1+(j+1)n+ja))\sum_{i=1}^{p} e^{\left(\frac{-(t-(t_1+(j+1)n+ja))}{\tau_i}\right)}] \tag{4.9}$$

Suppose that the time is $t = t_1+mn+ma$ (just before the beginning of the m^{th} wave)

Then, the equation takes the form;

$$P = \sum_{j=0}^{m-1} P_{0k} e^{-\sigma x} \left(e^{iw(t_1+(j+1)n+ja)} \sum_{i=1}^{p} e^{\left(\frac{-(t-(t_1+(j+1)n+ja))}{\tau_i} \right)} \right) \tag{4.34}$$

For simplicity take m=3, then,

$$\frac{P}{P_{0k}} = e^{-\sigma x} \left(e^{iw(t_1+n)} \sum_{i=1}^{p} e^{-\frac{(2n+3a)}{\tau_i}} + e^{iw(t_1+2n+a)} \sum_{i=1}^{p} e^{-\frac{(n+2a)}{\tau_i}} + e^{iw(t_1+3n+2a)} \sum_{i=1}^{p} e^{-\frac{a}{\tau_i}} \right) \tag{4.35}$$

Suppose that, the relaxation time that is wanted to be filtered is τ_1, then

$$\frac{P}{P_{0k}} = e^{-\frac{a}{\tau_1}} e^{-\sigma x} \left(e^{iw(t_1+n)} \sum_{i=1}^{p} e^{-\frac{(2n+3a)}{\tau_i}+\frac{a}{\tau_1}} + e^{iw(t_1+2n+a)} \sum_{i=1}^{p} e^{-\frac{(n+2a)}{\tau_i}+\frac{a}{\tau_1}} + e^{iw(t_1+3n+2a)} \sum_{i=1}^{p} e^{-\frac{a}{\tau_i}+\frac{a}{\tau_1}} \right) \tag{4.36}$$

Therefore, when "a"<<τ_i for $i \neq 1$then term in the exponent goes to zero or when "a">> τ_i for $i \neq 1$ then term in the exponent goes to minus infinity. Only the relaxation time which is in the same order with" a", is observed. Hence, by changing the PFR, corresponding relaxation times with "a" is filtered. This makes it possible to get relaxation time spectrum with "a".

4.4 Determination of Relaxation Time

Now, suppose that "a" has such a magnitude that only the relaxation time, τ is observed as explained in the spectral analysis part.

Hence, rearranging Equation 4.9 for just before the beginning of the 4th wave again,

$$\frac{P}{P_{0k}} = e^{-\frac{a}{\tau}} \left(e^{-\sigma x} e^{iw(t_1+n)} e^{-\frac{(2n+2a)}{\tau}} + e^{-\sigma x} e^{iw(t_1+2n+a)} e^{-\frac{(n+a)}{\tau}} + e^{-\sigma x} e^{iw(t_1+3n+2a)} \right) \tag{4.37}$$

Taking the natural logarithm of both sides;

$$\ln\frac{P}{P_{0k}} = -\frac{a}{\tau} + \ln\left[e^{-\sigma x} e^{iw(t_1+n)} e^{-\frac{(2n+2a)}{\tau}} + e^{-\sigma x} e^{iw(t_1+2n+a)} e^{-\frac{(n+a)}{\tau}} + e^{-\sigma x} e^{iw(t_1+3n+2a)} \right] \tag{4.38}$$

or in general form;

$$\ln\frac{P}{P_{0k}} = -\frac{a}{\tau} + \ln\left[\sum_{j=0}^{m-1} \left(K_{(m-1)-j} e^{-\frac{(j)(n+a)}{\tau_1}} \right) \right] \tag{4.39}$$

where

$$K_j = e^{-\sigma x} e^{iw(t_1+(j+1)n+ja)} \tag{4.40}$$

Taking the derivative with respect to "a"

$$\frac{d}{da}\left(\ln\frac{P}{P_{0k}} \right) = -\frac{1}{\tau_1} + \frac{\sum_{j=0}^{m-1} \left[K_{(m-1)-j} e^{\frac{-(j)(n+a)}{\tau_1}} \left(\frac{-j}{\tau_1} \right) \right]}{\sum_{j=0}^{m-1} \left[K_{(m-1)-j} e^{\frac{-(j)(n+a)}{\tau_1}} \right]} \tag{4.41}$$

The second term in the right hand side of the equation corresponds to superposition of recovery terms growing in number at the end of each signal. Here, if "n" is taken sufficiently large, all of the recovery terms except the final one become negligibly small, so second term in the equation goes to zero, then the equation reduces to,

$$\frac{d}{da}\left(\ln\frac{P}{P_{0k}} \right) \cong -\frac{1}{\tau_1} \tag{4.42}$$

Equation 4.42 can be used to obtain relaxation time of a viscoelastic solution through modulated ultrasound pulse measurements.

4.5 Relation between Complex Displacement, Density, Temperature and Pressure Amplitudes

To run simulations by using Equations 4.6, 4.7, 4.8 and 4.9, u_{0k}, ρ_{0k}, T_{0k} and P_{0k} should be specified. However, they cannot be arbitrarily specified since they depend on each other. Specifying of one these quantities the others are obtained spontaneously. In the ultrasonic experiments, the measured quantity is sound pressure or the echo amplitude rather than displacement, density or temperature. Hence, determination of u_{0k}, ρ_{0k} and T_{0k} in terms of P_{0k} is better for the simulations. Their relative magnitudes can be calculated by the following procedure.

Substituting the expressions for displacement, density and temperature variations in their continuous forms (Equation 4.1) into Equations 4.10, 4.11 and 4.12;

$$iw\rho_{0k} - iw\rho_0\sigma u_{0k} = 0 \tag{4.43}$$

$$-\rho_0 w^2 u_{0k} - K_T\alpha_V\sigma T_{0k} - L\sigma^2 u_{0k} = 0 \tag{4.44}$$

$$iwC_V T_{0k} - \frac{iwT\alpha_V K_T}{\rho_0^{\,2}}\rho_{0k} - \frac{k}{\rho_0}\sigma^2 T_{0k} = 0 \tag{4.45}$$

Hence, rearranging the equations, ρ_{0k} and T_{0k} are found in terms of u_{0k} as;

$$\rho_{0k} = \rho_0\sigma u_{0k} \tag{4.46}$$

$$\frac{(-\rho_0 w^2 - L\sigma^2)}{K_T\alpha_V\sigma}u_{0k} = T_{0k} \tag{4.47}$$

Finally, equation of motion can be used to relate P_{0k} with u_{0k}.

$$\rho_0\frac{\partial^2 u}{\partial t^2} = -\frac{\partial P}{\partial x} \tag{4.48}$$

Inserting Equation 4.6 and 4.9 into Equation 4.48 results in;

$$u_{0k} = -P_{0k} \frac{\sigma}{\rho_0 w^2} \tag{4.49}$$

CHAPTER 5

EXPERIMENTAL

5.1 Ultrasonic Measurements

In this work Ultrasound Doppler Velocimetry (UDV) system DOP2000 (Signal-Processing, Switzerland) is used. Many operating parameters such as ultrasound frequency, pulse reputation frequency and gate number can be adjusted by user. The experiments can be conducted in the ultrasound base frequencies of 0.5, 1.0, 2.0, 4.0 and 8.0 MHz. The pulse reputation frequency can be adjusted up to 15625 Hz. During the experiments the room temperature is kept as 25^0C. In the experiments, the piezzo ceramic transducer (SUHNER Switzerland RG 174/U 50 ohm) is immerged into 1L sample solution. The depth of the tip of the transducer is kept as 2 cm from the surface of the solution. The main parameter in the experiments is the PRF. Echo-history data with different PRF's are obtained to evaluate the mathematical model developed. Hence, echo amplitude versus time histories with various position data are recorded. 2.0, 3.0 and 4.0 wt % carboxy methyl cellulose (CMC) solutions are used as sample. CMC is taken from Sigma-Aldrich. Deionized water is used for the preparation of the CMC solutions. It is also obtained from Innovation Pure Water System.

Preparation procedure of CMC solutions is important since it is not easy to dissolve CMC in water. They are prepared by adding CMC into water in portions for well mixing. After the addition of CMC to water, the solution is mixed intermittently at 30^0C. Dissolution of CMC is completed after 2 days.

In addition, some properties of CMC taken from Sigma-Aldrich are given in Table 5.1.

Table 5.1 Properties of CMC

Property	Value
Molecular Weight	90 kDa
Degree of Polymerization	400
Degree of Substitution	0.65-0.90 (6.5-9.0 carboxymethyl groups per 10 anhydroglucose units)
Purity	99.5 % by weight

CMC is a derivative of cellulose consisting of carboxymethyl groups and its structure is shown in Figure 5.1.

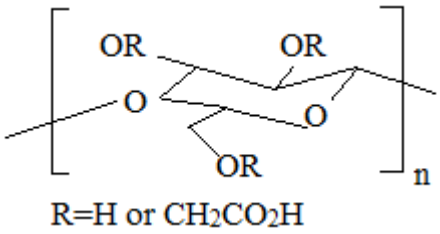

Figure 5.1 Repeating unit of CMC

The UDV devise also allows sound speed measurements by means of its dedicated accessory. Once defining the distance from the transducer end to the micrometric screw, the speed of sound in the liquid is measured. A detailed technical specification of the DOP2000 is given in Appendix A3.

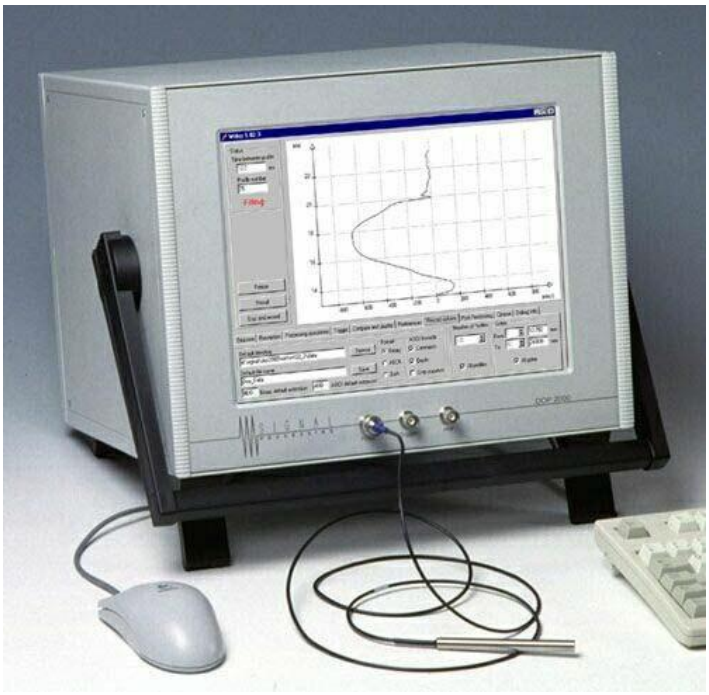

Figure 5.2 DOP2000 System

Although ultrasonic measurements on stationary fluids are not widely used, DOP2000 can also give important ultrasonic data. Applying the ultrasonic field measurement feature property, the attenuation coefficient can be obtained. In addition, amplitudes of the echoes coming from various times can be obtained by the DOP2000. By further evaluation of these echoes acoustic characterization of the material can be achieved. The relation between acoustic parameters and the material properties are developed and shown in the previous mathematical model derivation part.

5.2 Rheological Characterization

In order to evaluate the results obtained by the UDV measurements, the samples are also characterized by a well-established rheological measurement technique. These rheological measurements are done in METU Central Laboratory by ARES Rheometer (TA Instruments, Spain) (Figure 5.3). During the measurements, the device is operated in parallel plate mode at 25^0C. The diameters of the plates are 25 mm. By the rheometer creep experiments are

done on the CMC/water solutions. In these experiments, constant stresses (50 Pa) are applied on the samples. Thus, strain data with respect to time are collected. The obtained data are fitted to generalized Voigt-Kelvin model; hence, relaxation times according to model are obtained. The raw data obtained from the experiments are shown in the Appendix A.4.

Figure 5.3 ARES Rheometer (TA Instruments, Spain)

CHAPTER 6

RESULTS AND DISCUSSION

6.1 Analysis of Discrete Wave Propagation in Viscoelastic Medium by the Model Developed

In this part, on the basis of the model developed, numerical simulations are done to analyze the ultrasound propagation in a viscoelastic medium. In the simulations some physical properties of the hypothetical medium which are parameters in the model equation are listed in Table 6.1. Those values are similar to those of liquids. Furthermore, some ultrasonic experiments are also done to evaluate the results of the simulations.

Table 6.1 Physical properties of the hypothetical medium used in the simulations

Physical Property	**Value**
Density (ρ_0)	1000 kg / m^3
Temperature (T_0)	300 K
Thermal Conductivity (k)	0.5 W / m K
Constant Volume Heat Capacity (C_V)	5000 J / kg K
Isothermal Bulk Modulus (K_T)	10^9 Pa
Thermal Expansion Coefficient (α_v)	2.5×10^{-4} K^{-1}

First of all, behaviors of the media having different relaxation times (1.0 s, 0.1 s and 1.0×10^{-4} s) are simulated. The simulations are done with a base

ultrasonic frequency of 1 MHz, and the time between two consecutive pulse "a" (or PRF) is kept as 0.04s while pulse length, "n", is 0.05 s. The modulation of the applied ultrasound pulses are depicted in Figure 6.1.

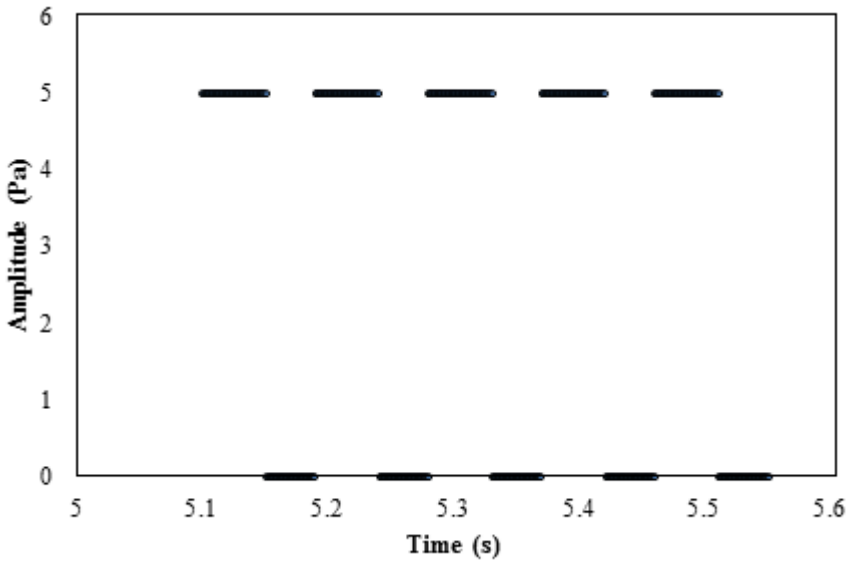

Figure 6.1 Modulation of the applied ultrasound pulses

In addition, all the physical properties except the relaxation time are constant. The response of the material to the applied ultrasound pulses are shown in Figures 6.2, 6.3 and 6.4 in terms of amplitude of sound pressure versus time.

When Figure 6.2 is analyzed, it represents discrete sound propagation in a medium having relaxation time of 1.0 s at a fixed position in the solution. The vertical axis shows the sound pressure and the horizontal axis represents the time. During the discrete sound propagation the medium is periodically compressed and then relaxed like a spring. The compression zone corresponds to the continuous propagation of wave. Then, the ultrasound pulse is stopped and relaxation of material starts. The duration of the compression and relaxation are determined by the pulse length and PRF of the sound. In the figure, material is compressed from the time 5.1 s to 5.15 s. Then, wave stops and material relaxes until the time 5.19 s. At this time new compression period starts. This trend continues during the application of the sound pulses.

From the figures it is seen that PRF and the relaxation time should be in the same order of magnitude to probe the relaxation phenomenon of the material. If PRF is much longer than the relaxation time as in Figure 6.4, the molecules come back to equilibrium position very fast so it gives inadequate monitoring of relaxation time. On the other hand, if PRF is much shorter than the relaxation time, the relaxation of the solution during this period will be insignificant, making it difficult to probe the variation of the pressure (Figure 6.2). It resembles a continuous wave propagation. However, when their magnitudes of the orders are similar, the relaxation of the material is clearly explored (Figure 6.3). Consequently, this method can be used to obtain relaxation time spectrum with different PRF's. Only the corresponding relaxation times with PRF are observed while the others are filtered. Hence, relaxation times in generalized viscoelastic models can be captured by changing the PRF.

In addition, pressure amplitude of the ultrasound is set to 5 Pa in simulations. For $\tau=1.0x10^{-4}$ s, the obtained pressure of sound is 5 Pa. In this case the solution relaxation time is much shorter than n which is 0.04 s. However, for τ= 0.1 s and 1.0 s, the peak sound pressures have not reached to 5 Pa yet. It requires longer "n" values to reach 5 Pa as for longer relaxation times mean slower response of the solution.

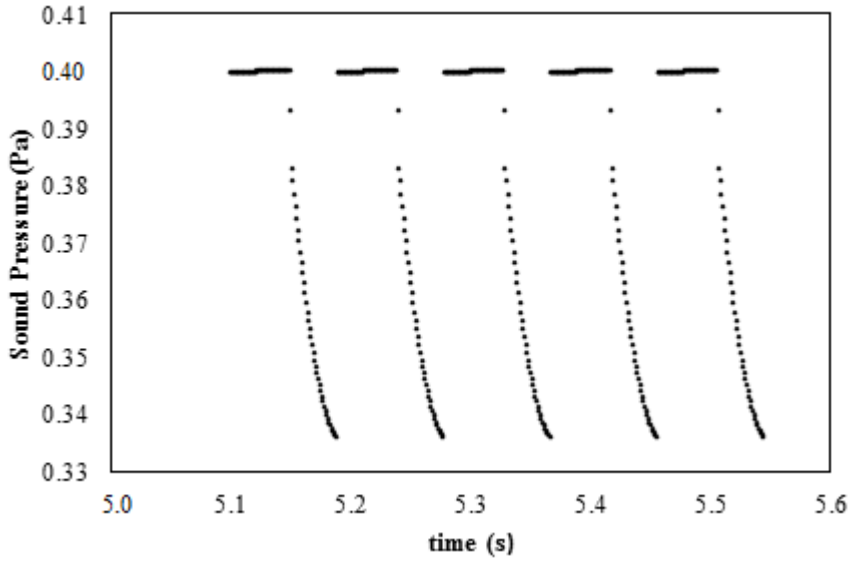

Figure 6.2 Sound pressure versus time for τ=1.0 s, f=1 MHz and PRF=0.04 s

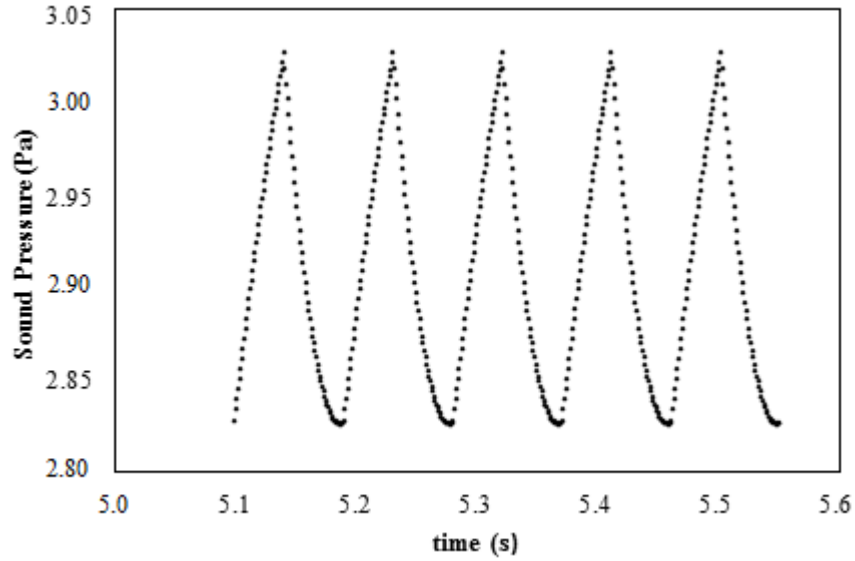

Figure 6.3 Sound pressure versus time for τ=0.1 s, f=1 MHz and PRF=0.04 s

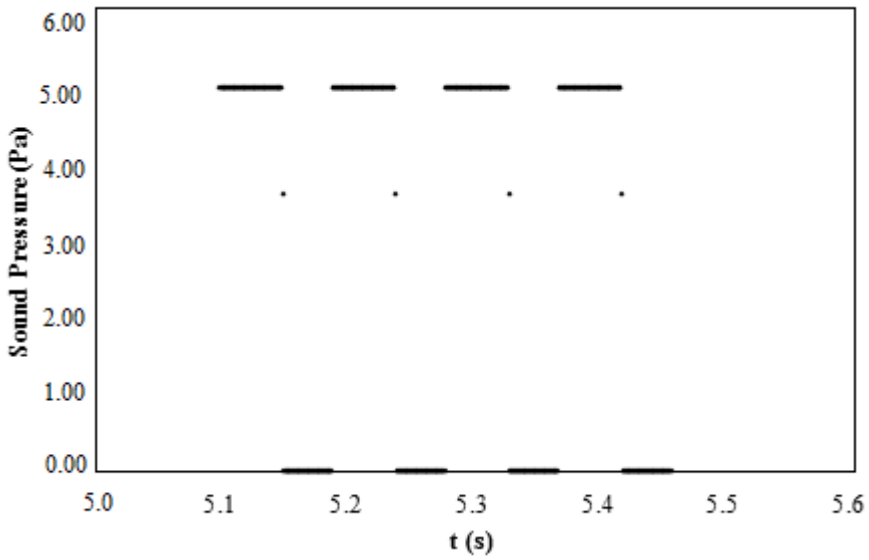

Figure 6.4 Sound pressure versus time for τ=1.0x10^{-4} s, f=1 MHz and PRF=0.04 s

Position dependency of the sound pressure amplitudes can also be examined by the model. Figures 6.2, 6.3 and 6.4 represent the results obtained at the point 1 cm from the transducer tip. When the sound pressure amplitudes are studied at different positions in the solution, it is seen that sound pressures gradually decreases with position. This is related with the attenuation of sound due to the viscous dissipation or the loss modulus. Figures 6.5, 6.6 and 6.7 show the sound pressure amplitudes from 2, 5 and 8 cm from the transducer end for τ=0.1s, f=1 MHz and PRF=0.04 s. These points lie on the axis of the transducer. The positions affects only the amplitude of the sound pressure while oscillation characteristics of the sound pressure remain constant as they are function of relaxation time of the solution and ultrasound pulse parameters of PRF and pulse length.

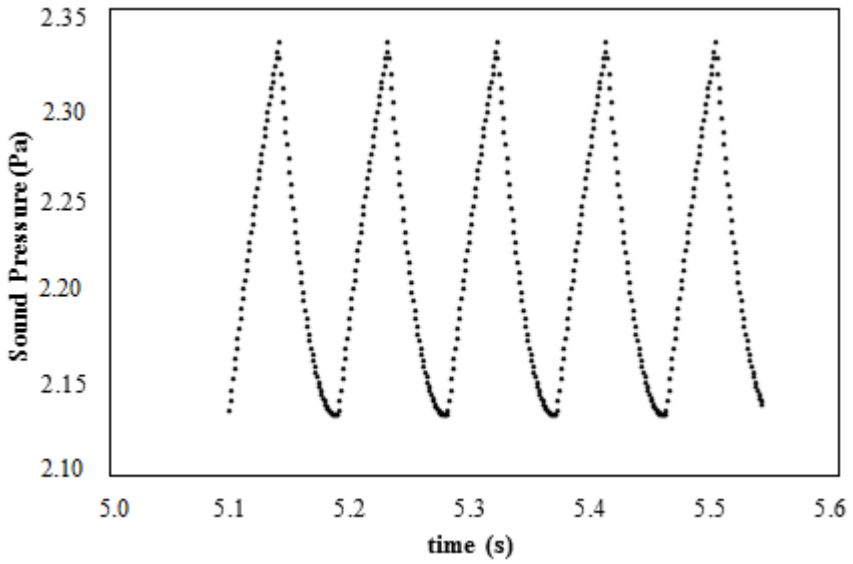

Figure 6.5 Sound pressure versus time for τ=0.1s, f=1 MHz and PRF=0.04 s at x=2 cm

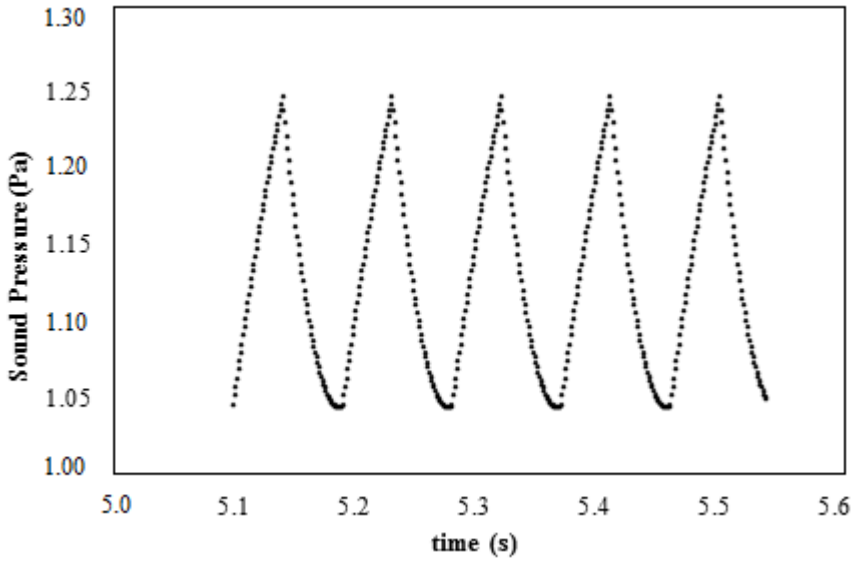

Figure 6.6 Sound pressure versus time for τ=0.1s, f=1 MHz and PRF=0.04 s at x=5 cm

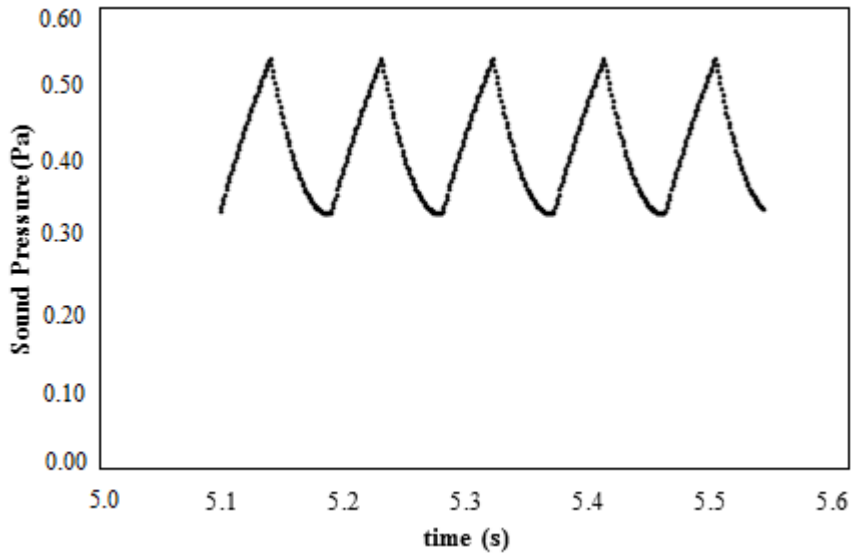

Figure 6.7 Sound pressure versus time for τ=0.1s, f=1 MHz and PRF=0.04 s at x=8 cm

Similar analysis can also be done for determining the frequency dependency of sound pressure level during discrete wave propagation. As in the position dependence, increasing the frequency decreases the sound pressure levels due to the sound attenuation. These results are given in Figures 6.8, 6.9 and 6.10 for 2, 4 and 8 MHz, respectively. It should be noted that, from the time point of view, the base frequency of the ultrasound has no effect relaxation of the sound pressure as the time scales involved are too different from each other. Here relaxation times of the solution in the order of milliseconds or seconds are considered while typical time scale of the ultrasound is in the order of 10^{-6} seconds. These are shown in Figures 6.8, 6.9 and 6.10. On the other hand, the UDV system allows one to modulate the pulses with pulse repetition frequencies in the range of the solution relaxation times.

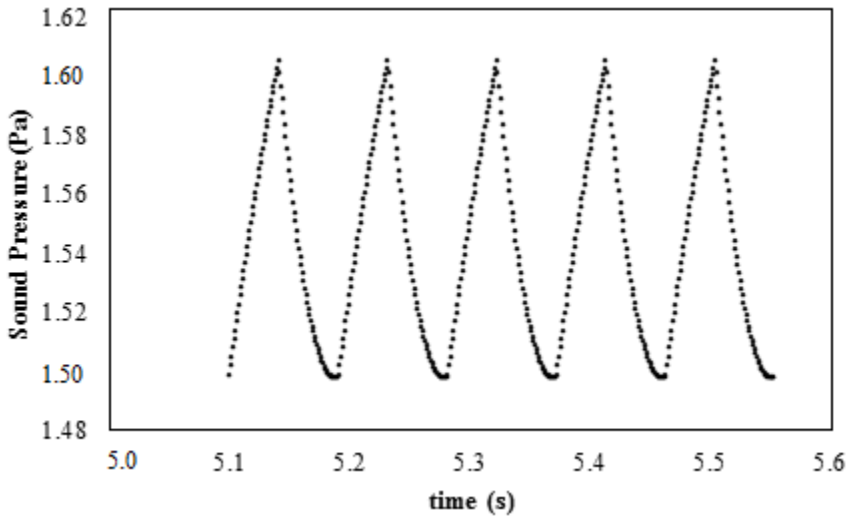

Figure 6.8 Sound pressure versus time for τ=0.1s, PRF=0.04 s for f=2 MHz

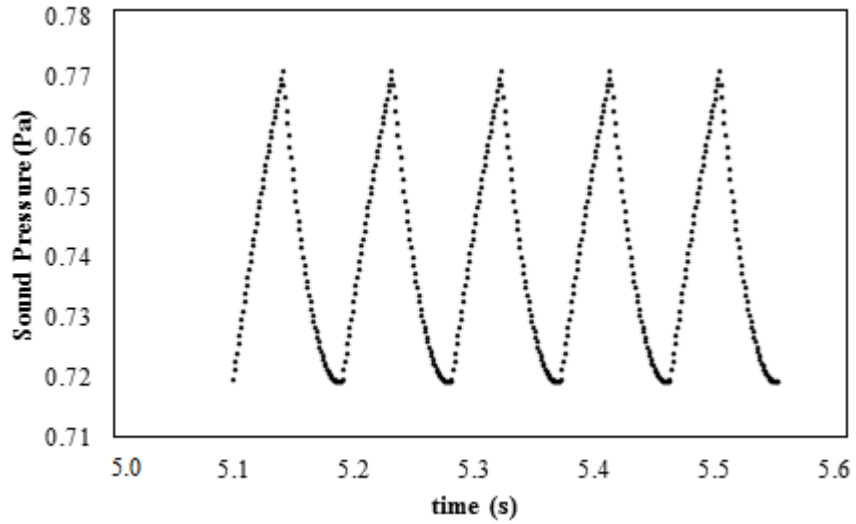

Figure 6.9 Sound pressure versus time for τ=0.1s, PRF=0.04 s for f= 4MHz

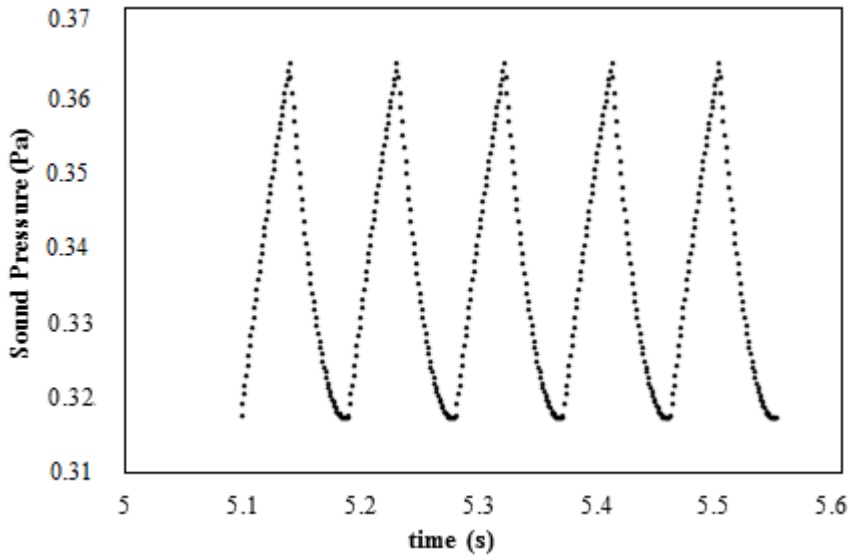

Figure 6.10 Sound pressure versus time for τ=0.1s, PRF=0.04 s for f= 8 MHz

6.2 Dependence of Sound Speed on the Acoustical Parameters and Material Properties

Sound propagation speed is another important parameter for the acoustical characterization techniques. Its dependence on ultrasound frequency, solution relaxation time and temperature are also analyzed through the simulations in which Equation 4.22 is employed. The properties of the hypothetical solution are listed in Table 6.1. In Figure 6.11 the effect of ultrasound base frequency up to 10 MHz on the sound speed are shown. The vertical axis is the sound speed and horizontal axis is the base frequency of the sound.

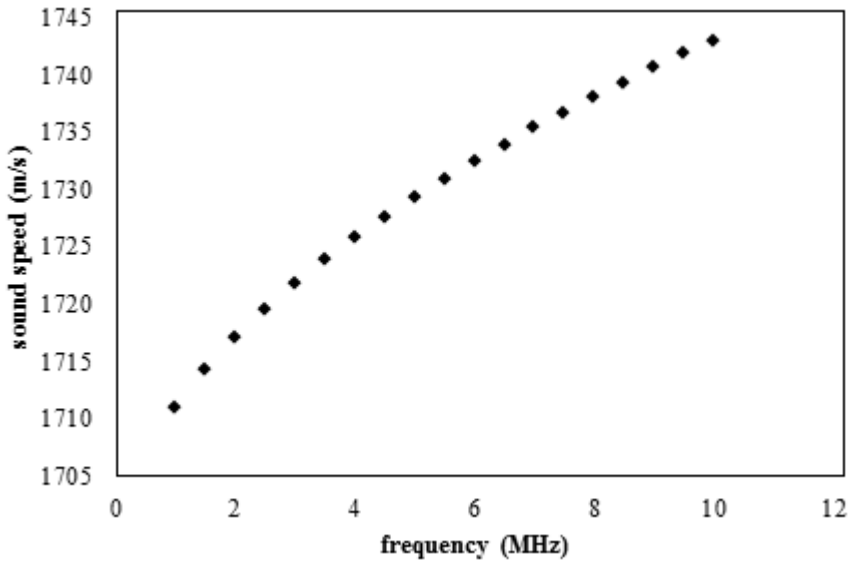

Figure 6.11 Sound speed versus frequency for τ=0.1s

It is seen that sound speed slightly increases with frequency. However, increase in the sound speed seems to be limited. Therefore, material characterization with a technique based on the sound speed dependent on ultrasound frequency is not promising. Experimental measurements for investigating the frequency dependency on sound speed are done with 2.0 wt. % CMC solution, as well. Figure 6.12 shows the experimental results of ultrasonic experiment done with CMC solution for determination of sound speed with frequencies from 1 MHz to 8 MHz. From the figure the sound speed is gradually increasing with frequency similar to the simulation results. The difference between the magnitudes of the sound speed obtained in the simulations and in the experiments stems from the differences between physical properties of assumed solution in the simulations and the CMC solution I the experiment. However, the trend of the sound speed variation with respect to the ultrasound frequency should be considered. From that respect simulations seems to capture sound speed versus ultrasound variations accurately.

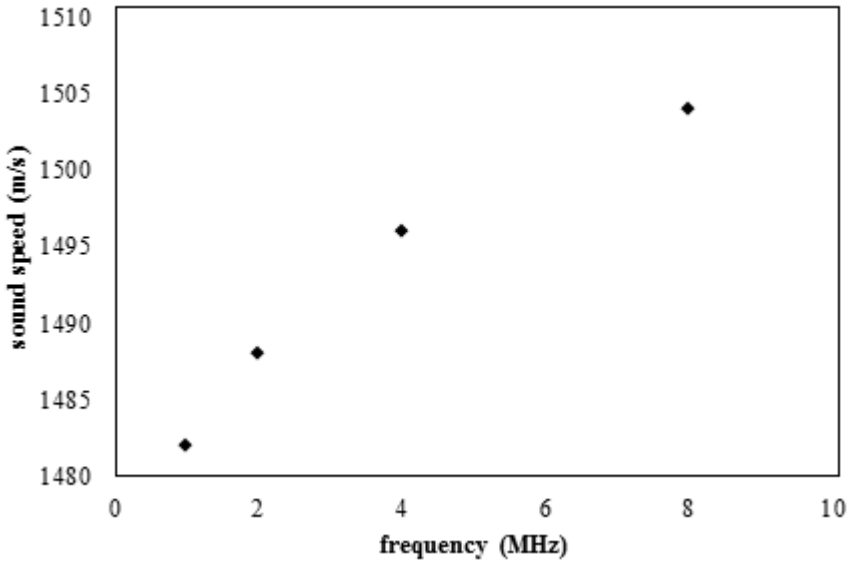

Figure 6.12 Sound speeds versus frequency for 2.0 wt. % CMC

On the other hand, the dependency of sound speed on the relaxation time of the material is more pronounced than on the ultrasound frequency. The simulations show that the sound speed decreases when the relaxation time of the material increases. Lower relaxation time means higher molecular stiffness that in turn means higher sound speeds compared to the a material with a shorter relaxation time. This behavior is observed in Figure 6.13. An exponential decay of speed with log τ is observed in the plot. The vertical axis is the sound speed and the horizontal axis is the logarithm of relaxation time on the base of ten.

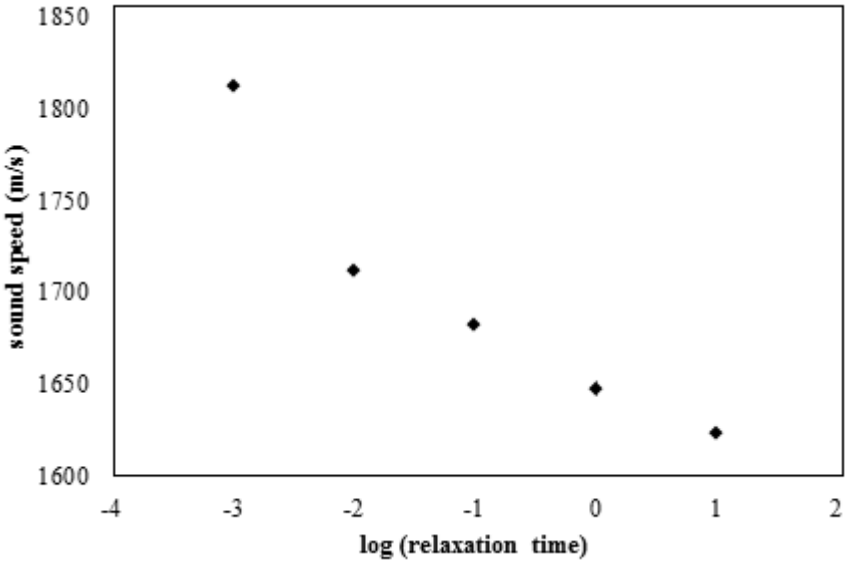

Figure 6.13 Sound speed versus $\log_{10}$ (relaxation time) f=1 MHz

This behavior can also be observed by the experimental sound speed measurements with different CMC concentrations. One term in the discrete relaxation time spectrums of the CMC solutions of 2.0 wt. %, 3.0 % and 4.0 % are 2417 μs, 3211 μs and 4953 μs, respectively. Those values are obtained by fitting conventional rheometer measurement results to the generalized Voigt-Kelvin constitutive rheological model. As the CMC in the solution gets lower, relaxation time of the solution also get lower, which is discussed in the coming part. Hence, sound speed decreases with the increase in the concentration of CMC in the solution. The experiments are done with base frequency of 1 MHz and the results are shown in Figure 6.14. The relaxation time range that could be obtained in the experiments is very narrow compared to the simulations. On the other hand, experimentally it is still possible to observe decreasing trend of the sound speed with respect to relaxation time. It should also be pointed out that, in the experiments the relaxation times were changed by changing the CMC composition of the solutions. This change in the composition could also affect speed of sound. As the concentration of the CMC was low, this possible effect has been neglected.

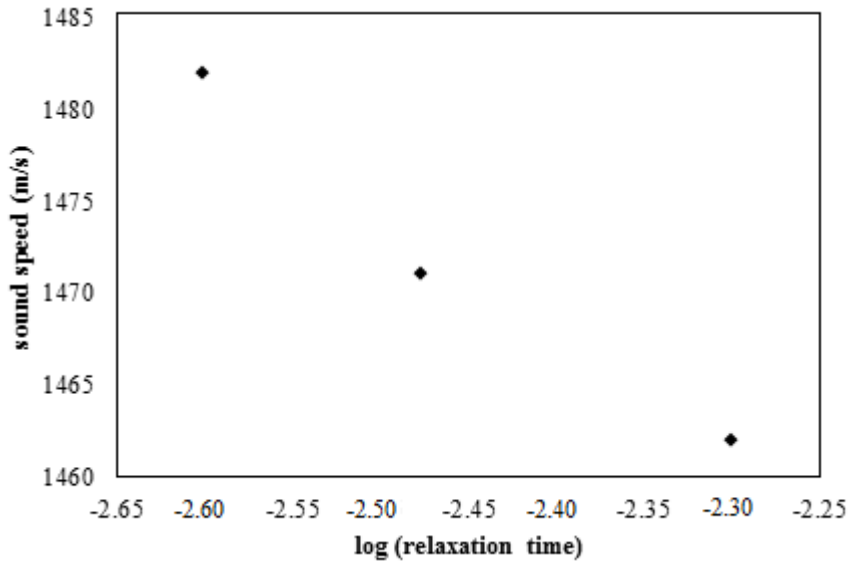

Figure 6.14 Sound speed versus various CMC relaxation times for f=1 MHz

Another parameter that might have a significant impact on the sound speed is temperature. In order to investigate the temperature effects simulations are carried out between 250 K and 360 K for the hypothetical solution introduced earlier. The results are shown in Figure 6.15. The vertical axis is the sound speed and the horizontal axis is the temperature. It is seen that sound speed decreases with temperature. This is mainly due that dynamic modulus decreases by temperature. Hence, sound speed is inversely proportional with temperature. Despite the considerable temperature variation, the change in the sound speed can be considered marginal. Hence for small temperature variations, i.e. few degrees, the sound speed can be considered constant.

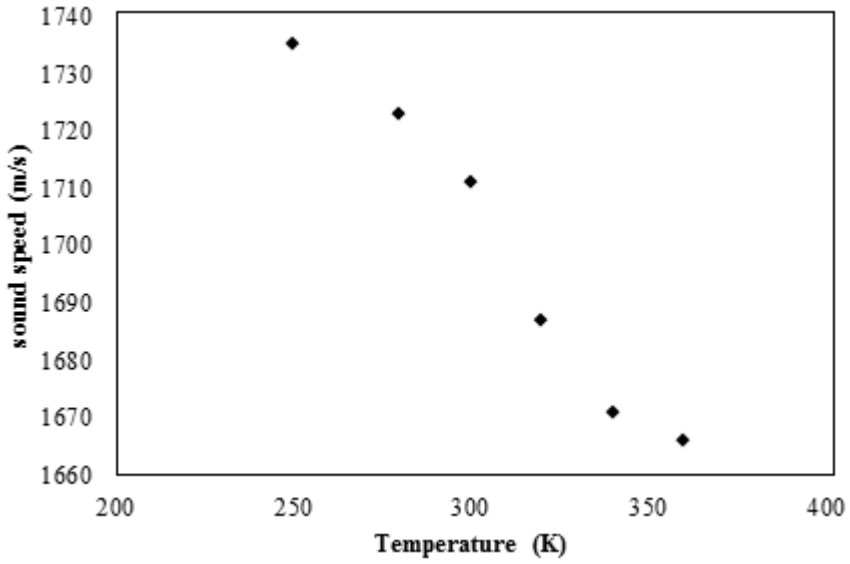

Figure 6.15 Sound speed versus temperature for τ=0.1s f=1 MHz

6.3 Relation between Sound Attenuation and the Material Properties

Sound attenuation is also important for the analyzing the sound propagation phenomena and commonly used in ultrasonic material characterization methods. It is strongly dependent on the frequency and material properties. It has already been demonstrated in Figures 6.8, 6.9 and 6.10 that the amplitude of ultrasound decreases with ultrasound frequency for a given location. This is an expected result since ultrasound at higher frequency is more prone to the scattering and other loss effects than that of lower frequency during while propagating in medium. In order to provide further insight on this effect, simulations and experimental measurements were carried out at different ultrasound base frequencies. The respective results are depicted in Figures 6.16 and 6.17 in the experiments 2.0 wt. % CMC solution was used. The figures show that attenuation gets higher as the ultrasound frequency increases since energy dissipation or loss modulus gets stronger in higher frequencies.

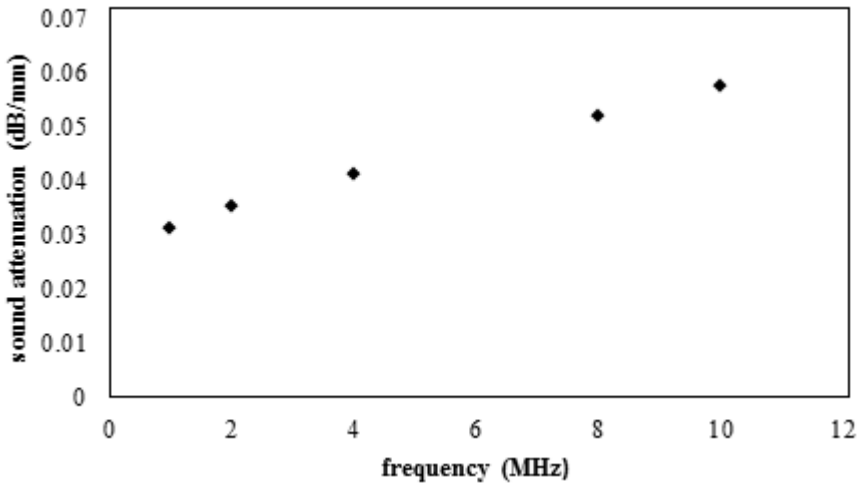

Figure 6.16 Sound attenuation with frequency for τ=0.1s

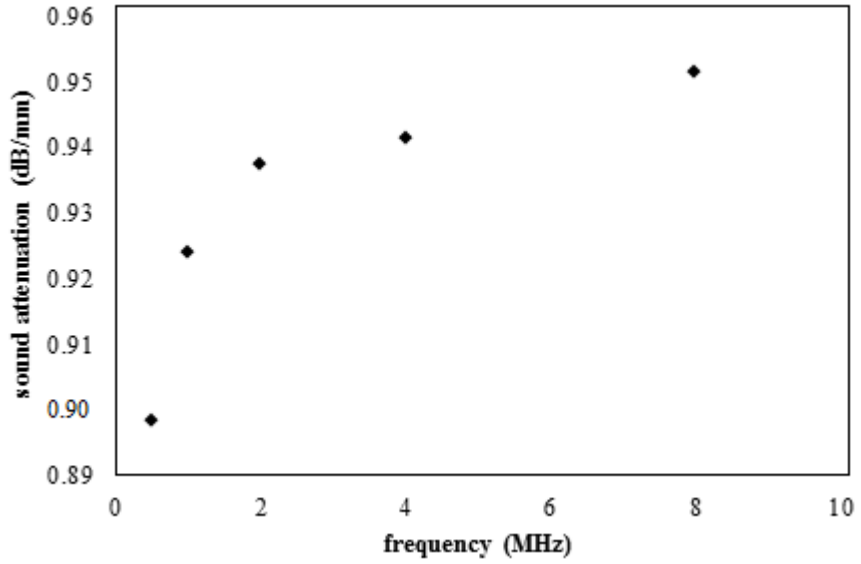

Figure 6.17 Sound attenuation with frequency for 2.0 wt. % CMC

Since, the attenuation is powerfully affected by the material properties, the attenuation with respect to different relaxation times are also plotted in Figure 6.18. As seen from the figure, it is increasing with the increase in relaxation times. In addition, experiments are done to analyze the relaxation time effect. Similar to the sound speed versus the relaxation time results shown in Figure 6.14, solutions at different relaxation times are obtained by changing the CMC composition as 2.0, 3.0 and 4.0 wt. %. Corresponding relaxation times are

2417 μs, 3211 μs and 4953 μs. As CMC concentration or relaxation time gets higher, the solution becomes more elastic and sound attenuation increases.

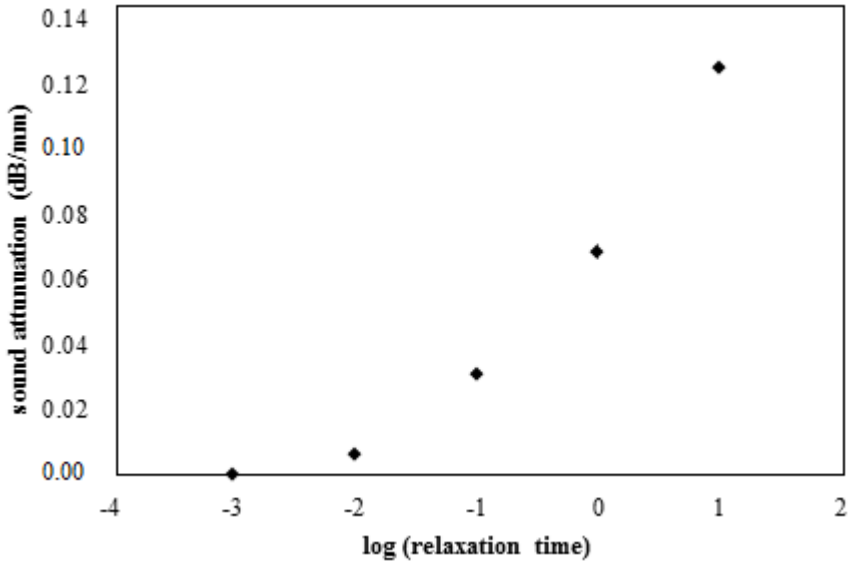

Figure 6.18 Sound attenuation with relaxation time for 1 MHz

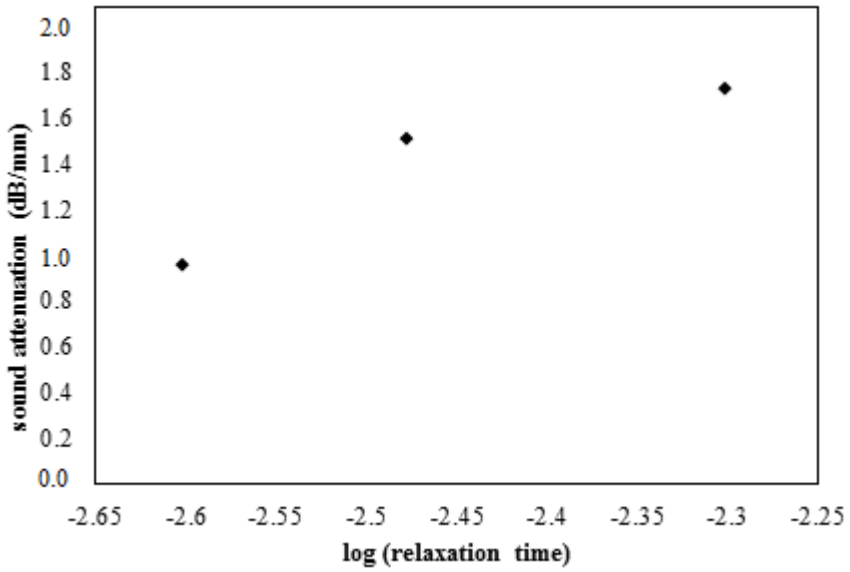

Figure 6.19 Sound attenuation with various CMC relaxation times for f=1 MHz

6.4 Analysis of the Temperature Variation in the Material

The model also helps to determine the temperature changes in the material due to the wave propagation. Since, the power of the sound is strongly dependent on the sound pressure; increasing the sound pressure level, the temperature variations can be expected to get more pronounced. However, the simulations show that these temperature variations are extremely small. The temperature changes with different ultrasound pressures are shown in Figure 6.20, 6.21 and 6.22. Even at the extreme sound pressure levels, temperature variations remain smaller than 0.1 K. Therefore it is safe to assume that the measurements are isothermal as far as the ultrasound effects are concerned.

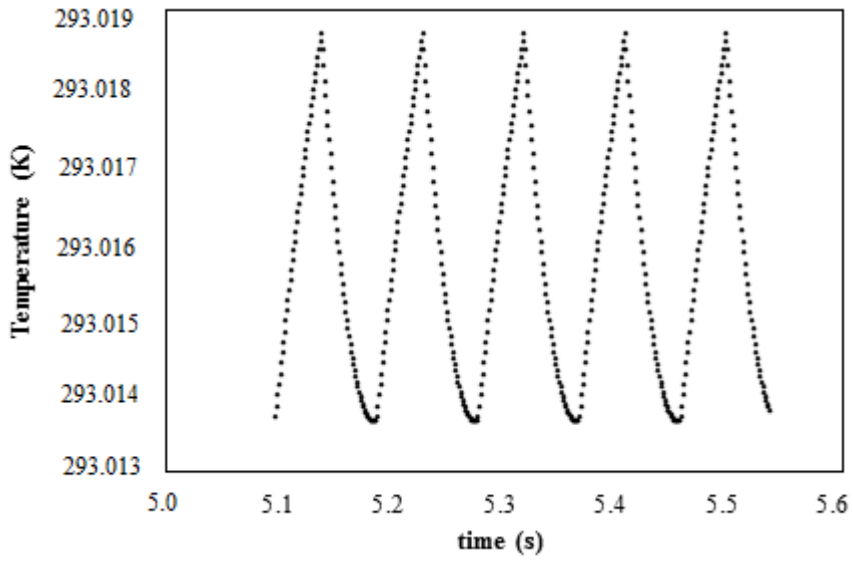

Figure 6.20 Temperature variation as a function of time for f=1MHz at 1 kPa

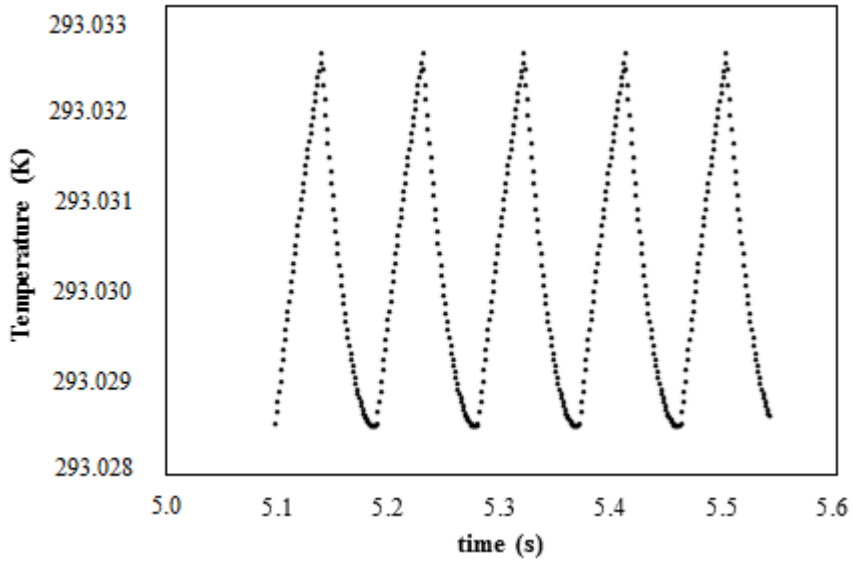

Figure 6.21 Temperature variation as a function of time for f= 1MHz at 1 MPa

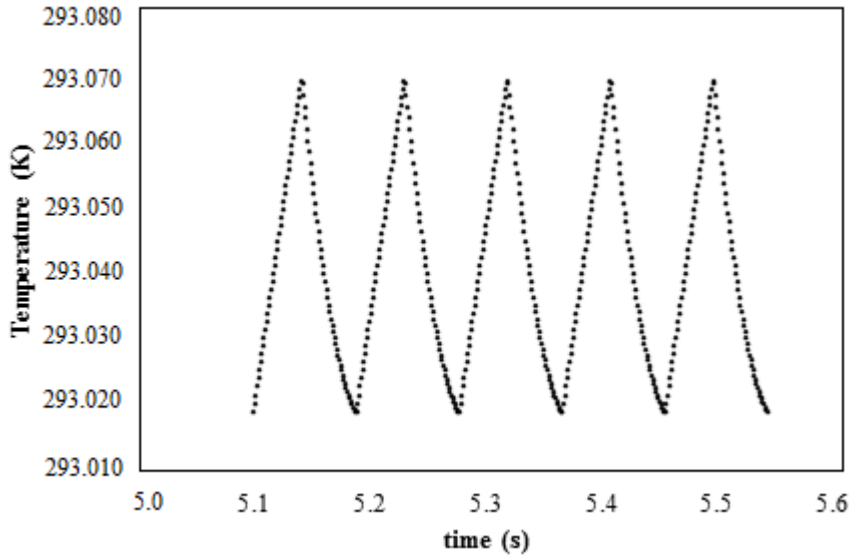

Figure 6.22 Temperature variation as a function of time for f=1MHz at 1 GPa

6.5 Determination of Relaxation Time

In the modeling Section 4.4, it has been shown that by using appropriate modulated ultrasound pulses, it is possible to measure relaxation time of viscoelastic materials by ultrasonic measurements. Making the "n" sufficiently long, superposition terms coming due to the previous waves

becomes negligibly small, as shown in Section 4.4. It is shown in Section 4.4 that the slope of the decay in the sound pressure amplitude with respect to "a" is inversely proportional to the relaxation time as $-\frac{1}{\tau}$.

In the data acquisition mode of the DOP2000, the amplitude of the echoes just beginning of a wave can be obtained; hence, the relaxation time can be obtained by evaluating the experimental data with different "a" values. However, real viscoelastic materials, e.g. polymer solutions, have many relaxation times originating from different configurations and interactions among the chains. As stated earlier, by varying "a" relaxation times with similar magnitudes can be probed. Thus, changing the order of magnitude of "a", the relaxation time that corresponds to the same magnitude of "a" is filtered. Eventually, spectrum of relaxation time can be achieved. DOP2000 is capable of generating pulses having repetition frequency between 64 μs and 10500 μs. To obtain the spectrum, the ultrasonic experiments are done with three different magnitude of "a". "a" values are set as 65-90 μs, 650-900 μs and 6500-9000 μs. Experiments are done with 2,0 wt. %, 3,0 wt. % and 4,0 wt. % CMC solutions. From the data acquired, natural logarithms of sound amplitude versus "a" graphs are drawn. For Figure 6.23, the vertical axis is the natural logarithm of the sound pressure amplitude of the received signal and the horizontal axis represents the time "a". It is seen that linear relation is held. The slope of the graph corresponds to $-\frac{1}{\tau}$ and the intercept is related with the base frequency of the ultrasound. Numerous experiments are done and ultrasonic data acquired are consistent. The standard deviations for the evaluation of the experimental data are less than 0.1. In the figures arithmetic mean of the data are used.

Figures 6.23, 6.24 and 6.25 belong to the experimental measurements done with a=65-90 μs. Hence, the relaxation time corresponding to this magnitude

is filtered. From the figures it is seen that the slopes of the plots are decreasing by increasing the concentration. Hence, increasing the concentration of CMC in the solution raises the elasticity of the solution. The relaxation times are found as 64.5 μs, 78.7 μs and 81.9 μs for the CMC solutions of 2.0 wt. %, 3.0 wt. % and 4.0 wt. % respectively. Furthermore, the empirical models developed for the prediction of viscoelasticity of polymeric solutions also suggest that the viscoelasticity of solutions should increase with the concentration of the polymer [40].

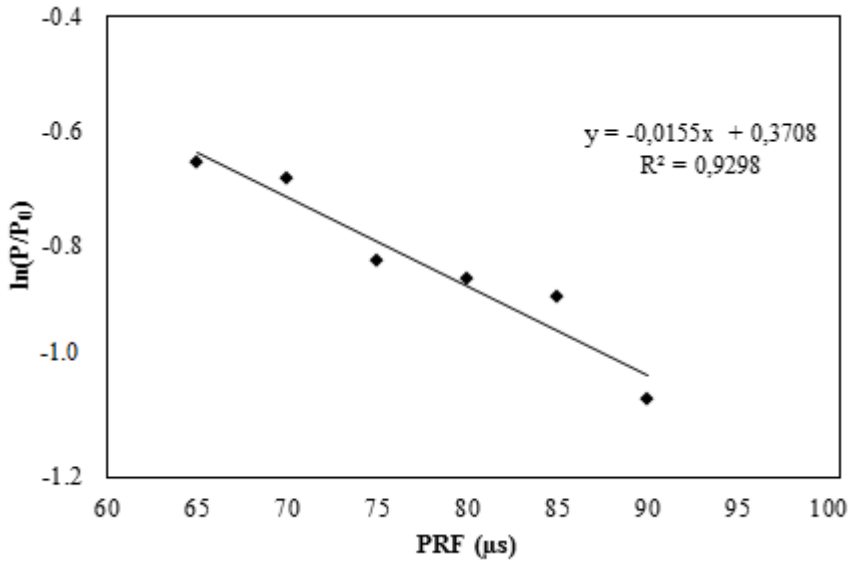

Figure 6.23 $\ln(P/P_0)$ versus a for 2.0 wt. % CMC solution at f=1MHz for PRF = 65-90 μs

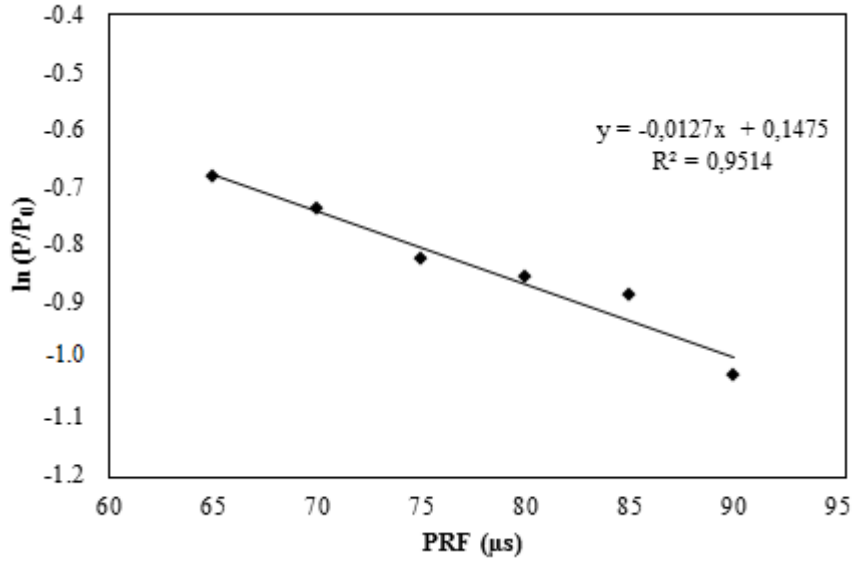

Figure 6.24 ln(P/P_0) versus a for 3.0 wt. % CMC solution at f=1MHz for PRF = 65-90 µs

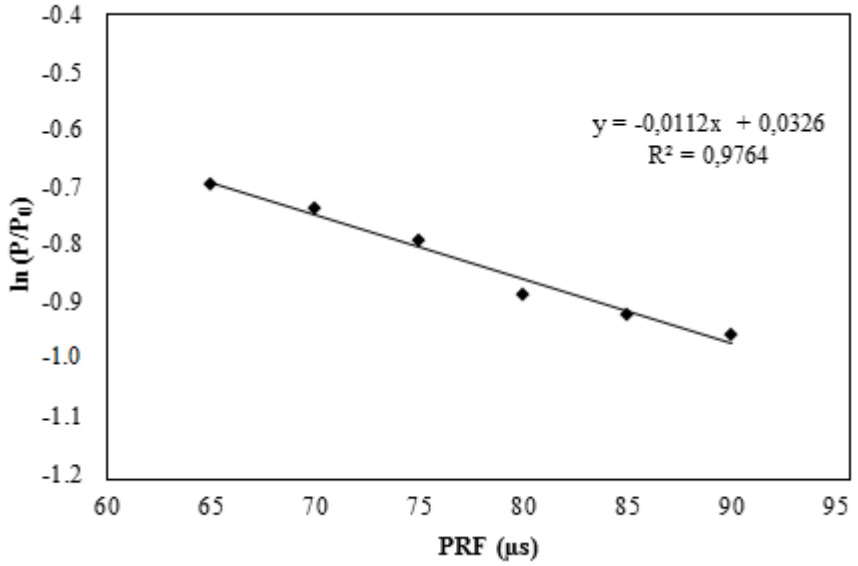

Figure 6.25 ln(P/P_0) versus a for 4.0 wt. % CMC solution at f=1MHz for PRF = 65-90 µs

In addition, results of the similar experiments done with a=650-900 µs are shown in Figures 6.26, 6.27 and 6.28. The relaxation times are obtained as 312.5 µs, 454.5 µs and 526.3 µs for the CMC solutions of 2.0 wt. %, 3.0 wt. % and 4.0 wt. % respectively. The results of the experiments for a=6500-9000

μs are presented in Figures 6.29, 6.30 and 6.31. The relaxation times are obtained as 2500 μs, 3333 μs and 5000 μs for the CMC solutions of 2.0 wt. %, 3.0 wt. % and 4.0 wt. % respectively.

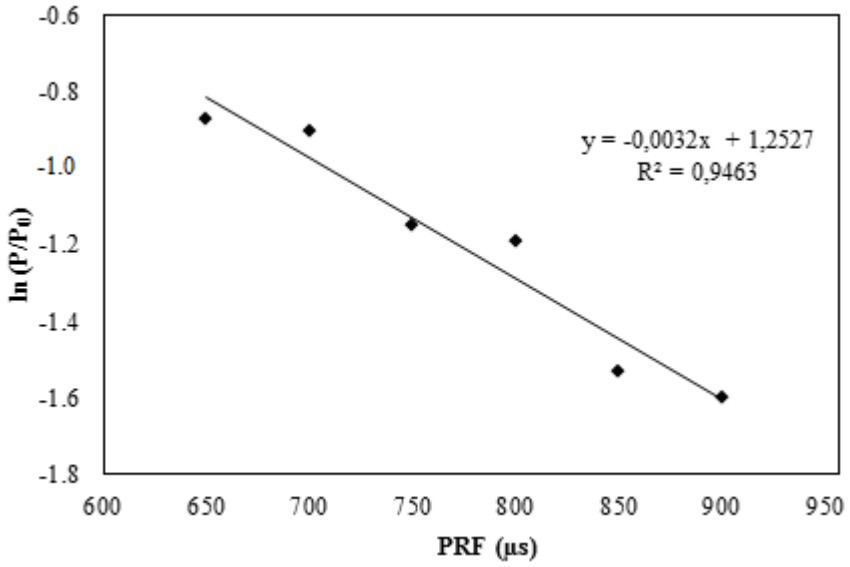

Figure 6.26 ln(P/P_0) versus a for 2.0 wt. % CMC solution at f=1MHz for PRF = 650-900 μs

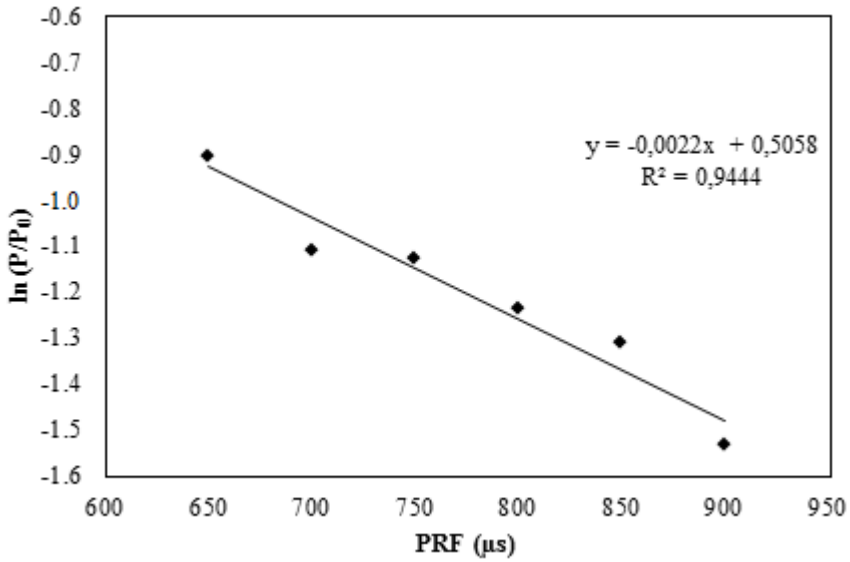

Figure 6.27 $\ln(P/P_0)$ versus a for 3.0 wt. % CMC solution at f=1MHz for PRF = 650-900 µs

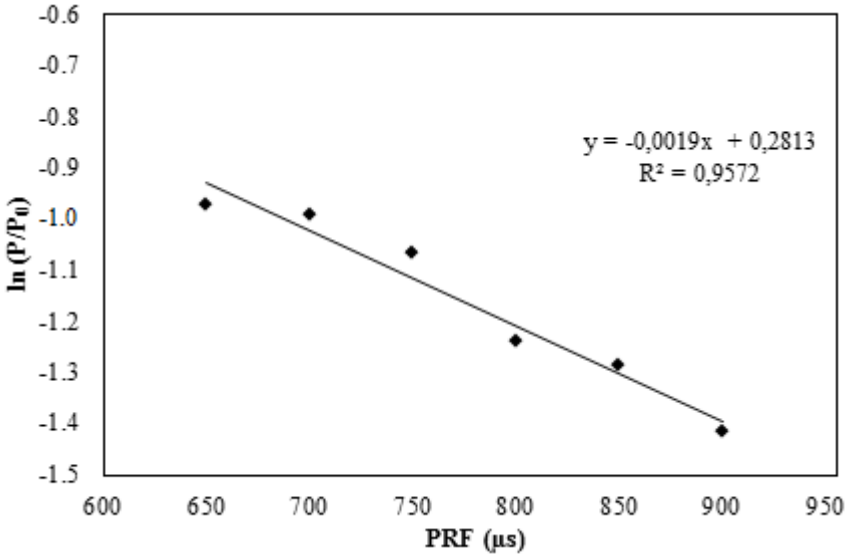

Figure 6.28 $\ln(P/P_0)$ versus a for 4.0 wt. % CMC solution at f=1MHz for PRF= 650-900 µs

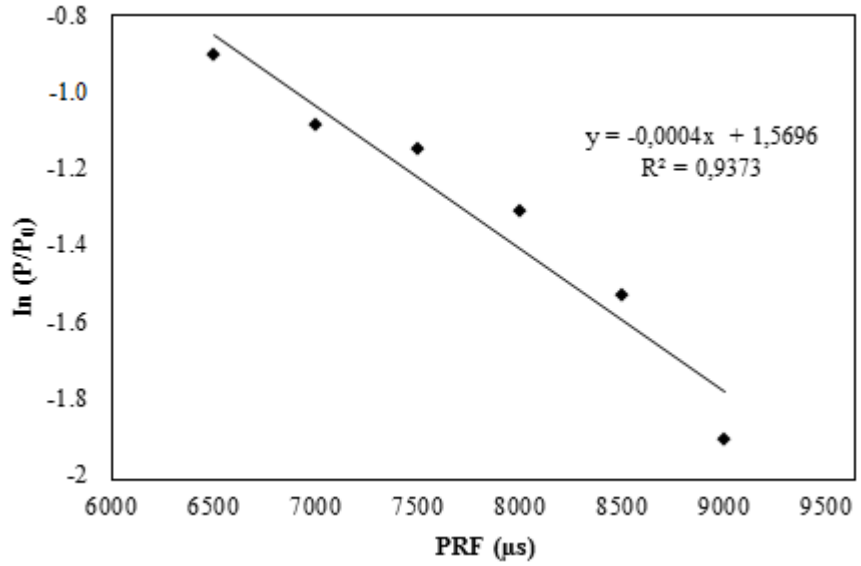

Figure 6.29 ln(P/P_0) versus a for 2.0 wt. % CMC solution at f=1MHz for PRF = 6500-9000 µs

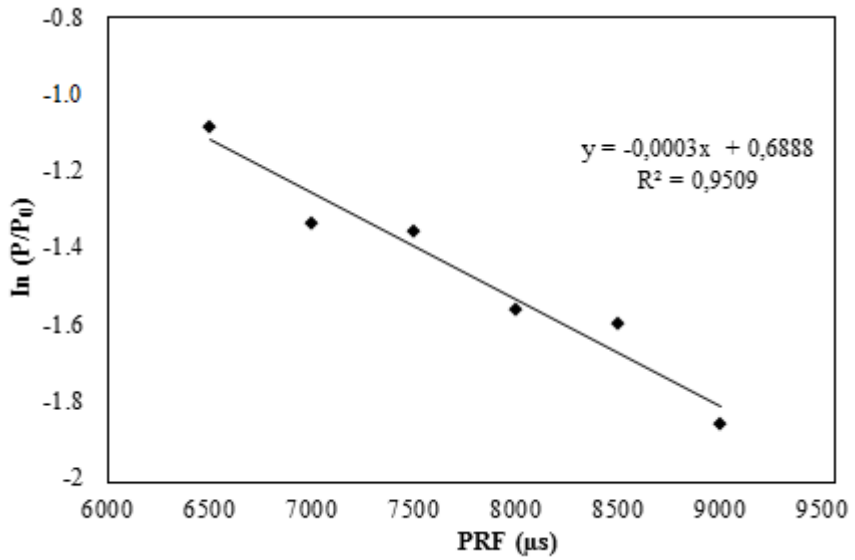

Figure 6.30 ln(P/P_0) versus a for 3.0 wt. % CMC solution at f=1MHz for PRF = 6500-9000 µs

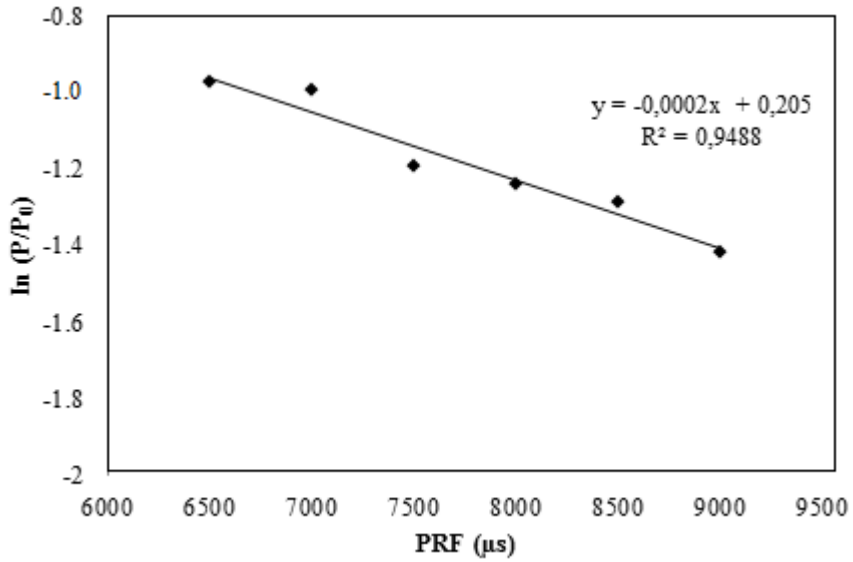

Figure 6.31 $\ln(P/P_0)$ versus a for 4.0 wt. % CMC solution at f=1MHz for PRF = 6500-9000 µs

6.6 Rheometer Experiments

Dynamic mechanical testing of polymers is also done for the solutions by TA Instruments ARES Rheometer. The data obtained from the rheometer experiment is fitted to generalized Voigt-Kelvin model. Use of four terms is concluded to express the experimental results sufficiently enough. The Voigt-Kelvin model parameters for the CMC solutions are tabulated in Table 6.2.

Table 6.2 Linear viscoelastic parameters in generalized Voigt-Kelvin Model for CMC/water solutions

	2.0 wt.% CMC		**3.0 wt.% CMC**		**4.0 wt.% CMC**	
m	**λ_m (µs)**	**η_m (Pas)**	**λ_m (µs)**	**η_m (Pas)**	**λ_m (µs)**	**η_m (Pas)**
1	2417	271	3211	370	4953	534
2	302	13	441	13	521	15
3	59	6	82	8	90	9
4	1	1	2	1	3	1

In Table 6.2 “m” represents the corresponding Voigt-Kelvin parameter. The rheometer results show that first three terms in the generalized Voigt-Kelvin model of CMC solutions are close to ultrasonic measurements. Since the magnitude of PRF falls in the range of the terms in the model, they are filtered while the remaining terms are discarded. Hence, this makes it possible to obtain discrete relaxation spectrum, by changing the magnitude of PRF. Accuracy of ultrasonic results can be accepted to be high. Since, the ultrasonic results deviates from the rheometer results no more than 10%. For qualitative ultrasonic measurements, results of the measurements can be corrected by calibration from the rheometer results. The comparison of rheometer results and ultrasound results are given in Figures 6.32, 6.33 and 6.34.

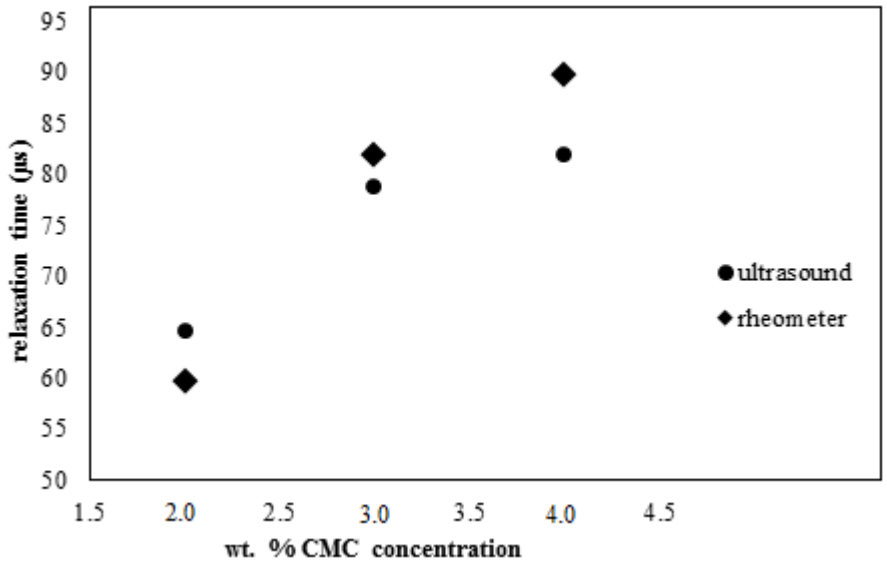

Figure 6.32 Comparison of rheometer measurements and corresponding ultrasound measurements for a = 65-90 µs

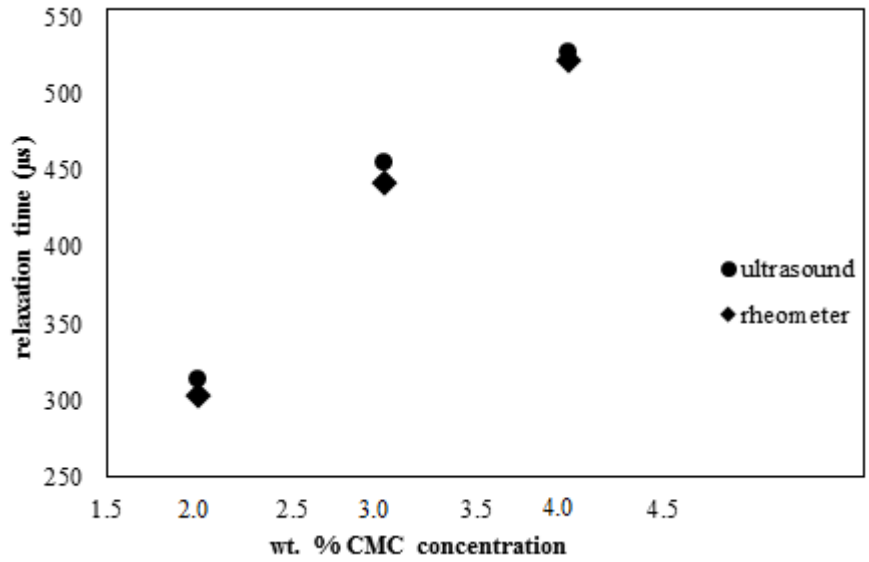

Figure 6.33 Comparison of rheometer measurements and corresponding ultrasound measurements for a = 650-900 µs

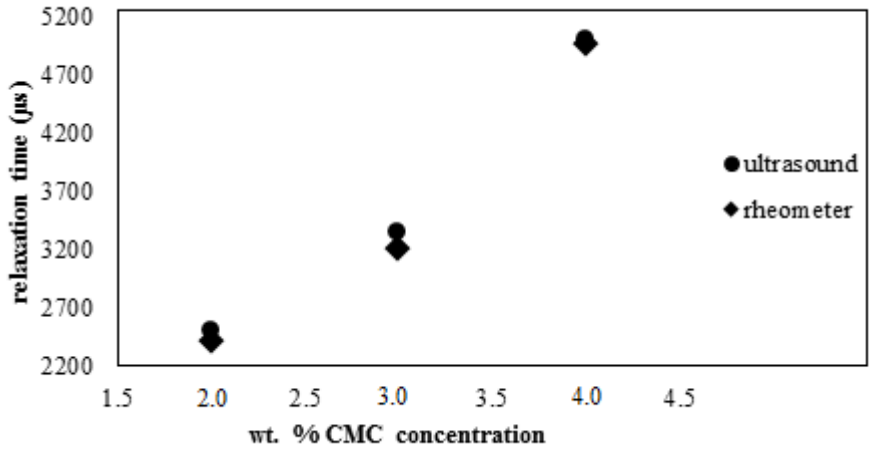

Figure 6.34 Comparison of rheometer measurements and corresponding ultrasound measurements for a = 6500-9000 µs

CHAPTER 7

CONCLUSIONS

In this study, discrete sound wave propagation in viscoelastic medium is investigated to probe its viscoelastic properties. For this purpose a mathematical model relating the discrete wave propagation with the material properties is developed. In the model heat effect due to viscous dissipation during the sound propagation is also included. On the basis of the model developed numerical simulations are done to visualize the sound propagation.

The simulations mainly deal with sound pressure variation with time under different conditions. It is seen that pressure change looks like spring. During wave propagation, pressure increases like compression. When the wave stops, then pressure decreases as decompression. Relaxation time is very critical parameter determining these increase and decrease trends. If the relaxation time is much higher when compared with the pulse repetition frequency, material does not have enough time to relax during PRF; hence, discrete wave propagation resembles to a continuous wave propagation. Material behaves like a perfectly elastic material. When the relaxation time of the material and PRF are close to each other, relaxation of the material is clearly observed during the period of PRF. However, if the relaxation time is much smaller than PRF, then material immediately relaxes when wave stops. This results in that no relaxation behavior is observed. Material behaves like perfectly inelastic body. Hence, PRF is an important for the detection of relaxation time. Hence, changing the time between two consecutive pulses the corresponding

relaxation times in the generalized viscoelastic models can be filtered. This makes it available to obtain relaxation time spectrum. Furthermore, the model imposes that a linear relation exists between natural logarithm of sound pressure amplitude and the time PRF.

The change in the sound pressure with different positions and frequencies are also simulated. Besides, sound speed and attenuation is also calculated from the model for different operating conditions. Furthermore, heat effect is concluded to be negligibly small as results of simulations. Ultrasonic measurements by DOP2000 are also done to examine the results of the simulations by 2.0 wt., 3.0 wt., and 4.0 wt. % CMC/water solutions. In these measurements, three different ranges of PRF are used; 65-90 μs, 650-900 μs and 6500-9000 μs. For each range, the relaxation time which has similar magnitude with PRF is probed. Hence, three terms in the discrete relaxation spectrum are obtained. In addition, for comparison, the rheological properties of the solution are also investigated with TA Instruments ARES Rheometer . The rheological data are fitted to generalized Voigt-Kelvin model having four terms. Finally, for the range of PRF = 65-90 μs, the relaxation times are determined as 64.5 μs, 78.7 μs and 81.9 μs for 2.0 wt. %, 3.0 wt. % and 4.0 wt. % CMC solutions, respectively. The corresponding results of the rheometer are 59.7 μs, 81.9 μs and 89.8 μs for 2.0 wt. %, 3.0 wt. % and 4.0 wt. % CMC solutions, respectively. When the range of PRF is set between 650 and 900 μs, the relaxation terms are obtained as 312.5 μs, 454.5 μs and 526.3 μs for 2.0 wt. %, 3.0 wt. % and 4.0 wt. % CMC solutions, respectively. The rheometer results for this magnitude are 302.5 μs, 441.1 μs and 521.3 μs for 2.0 wt. %, 3.0 wt. % and 4.0 wt. % CMC solutions, respectively. For the values of PRF between 6500 μs and 9000 μs, the relaxation times are probed as 2500 μs, 3333 μs and 5000 μs for 2.0 wt. %, 3.0 wt. % and 4.0 wt. % CMC solutions, respectively. The rheometer results come out as 2417 μs, 3211 μs and 4953 μs for 2.0 wt. %, 3.0 wt. % and 4.0 wt. % CMC solutions,

respectively. The ultrasonic measurements and rheometer results slightly deviate from each other. Hence, corrected results can be obtained from the calibration of the ultrasonic measurements.

REFERENCES

[1] P.P. Nanekar and B. K. Shah 2003. Characterization of Material Properties by Ultrasonics. BARC Newsletter, 249, 25-38.

[2] Bret A. Martin, Stuart W. Wenzel, Richard M. White 1989. Viscosity and Density Sensing with Ultrasonic Plate Waves. Sensors and Actuators A: Physical, 22(1-3), 704–708.

[3] Jens Blauert, Ning Xiang 2009. Acoustics for Engineers: Troy Lectures. Springer, Bochum, Germany.

[4] P. Zhao, J. Z. Fu And S. B. Cui 2011. Non-Destructive Characterisation of Polymers During Injection Moulding with Ultrasonic Attenuation Measurement. Materials Research Innovations, 15(1), 311-314.

[5] John Homer, Mark J Howard, Susan C Gooda 2000. Effect of Ultrasound on Molecular Mobility in Certain Crystalline Compounds. Ultrasonics Sonochemistry 2(2), 71-74.

[6] Oudina Assia and Djelouah Hakim 2010. Propagation of Ultrasonic Waves in Viscous Fluids. Wave Propagation in Materials for Modern Applications, 293-306.

[7] Lijuan Zhao, Zhigang Sun, Jacques Tatibouet, Shaoyun Guo 2009. Ultrasonic Characterization of the Crystallization Behavior of Poly(ethylene terephtalate. Journal of Applied Polymer Science, 114(5), 2731-2739.

[8] I Perepechko 1975. Acoustic Methods of Investigating Polymers. Mir Publishers, Moscow.

[9] Dharmendra Kumar Pandey and Shri Pandey 2010. Ultrasonics: A Technique of Material Characterization. Acoustic Waves 397-431.

[10] Shan Wang,Congmei Lin, Huimin Sun,Fan Chen, Jiang Li,Shaoyun Guo 2012. Ultrasonic Characterization of Phase Morphology of High Density

Polyethylene/Polyamide 6 Blend Melts. Polymer Engineering and Science 52(2), 338-345.

[11] Pascal Laugier and Guillaume Haïat 2011. Introduction to the Physics of Ultrasound. Springer, Paris, France.

[12] Gómez Álvarez-Arenas 2002. Longitudinal and Shear Wave Propagation in Silica Aerogels at Ultrasonic Frequencies. Instituto de Acústica del CSIC, Madrid, Spain.

[13] Antonio Almeida Silva, Edgard De Macedo Silva, Victor Hugo C. De Albuquerque, João Manuel R. S. Tavares 2009. Microstructural Characterization of Carbon Steels Using Ultrasonic Velocity Measurements. 20th International Congress of Mechanical Engineering, Gramado, RS, Brazil.

[14] Mason, W. P. (Ed.), Mcskimin, H. J. 1964. Physical Acoustics vol. 1A. In Academic, New York.

[15] Stephen L. Rosen 1993. Fundamental Principles of Polymeric Materials Second Ed.. John Wiley & Sons.

[16] Laura J. Pyrak-Nolte,Suyong Lee,Osvaldo Campanella 2004. Determination of Ultrasonic-Based Rheological Properties of Dough During Fermentation. Journal of Texture Studies, 35, 33-51.

[17] R.M. Christensen 1982. Theory of Viscoelasticity An Introduction Second Ed.. Academic Press.

[18] Oscar Sotolongo Costa, Alexei Vázquez Vázquez, and José Marín Antuna 1997. Influence of Viscoelastic Properties on The Propagation of Small Amplitude Sound Waves. Brazillian Journal of Physics, 27(3), 379-382.

[19] Jennifer N. Perkins and Tyler M. Lach. 2011. Viscoelasticity : Theories, Types, and Models. Nova Science Publishers.

[20] Hillesheim, Heather 2012. Sound and Light. New York NY : Infobase Learning.

[21] Hessen, B 1931. The Social and Economic Roots of Newton's 'Principia'. In Science at the Crossroads, 147-212.

[22] S. Parthasarathy M. Pancholy 1956. Sound Propagation in Liquids. Annalen der Physik, 452(6-8), 417-422.

[23] Francesca Lionetto, Alfonso Maffezzoli 2009. Polymer Characterization by Ultrasonic Wave Propagation. Advances in Polymer Technology, 27(2), 63-73.

[24] R.B. Bird, W.E. Stewart and E.N. Lightfoot 2002. Transport Phenomena Second Ed.. John Wiley & Sons.

[25] R. Byron Bird, Robert C. Armstrong, Ole Hassager 1987. Dynamics of Polymeric Liquids Volume 1: Fluid Mechanics, Second Ed.. John Wiley& Sons.

[26] W.L. Mccabe, J.C. Smith and P. Harriott 2005. Unit Operations of Chemical Engineering Seventh Ed.. McGraw Hill.

[27] Richard A. Pethrick, Dunbeath : Whittles 2010. Polymer Science and Technology for Scientists and Engineers. John Wiley & Sons.

[28] Hal F.Brinson, L. Catherine Brinson 2008. Polymer Engineering Science and Viscoelasticity: An Introduction. Springer.

[29] Montgomery T. Shaw, William J. Macknight 2005. Introduction to Polymer Viscoelasticity Third Ed.. John Wiley & Sons.

[30] John D. Ferry 1980. Viscoelastic Properties of Polymers, 3rd Ed.. John Wiley & Sons.

[31] William N. Findley, James S. Lai and Kasif Onaran 1989. Creep and Relaxation of Nonlinear Viscoelastic Materials with an Introduction to Linear Viscoelasticity. Dover Publications, New York.

[32] Malcolm J. W. Povey 1997. Ultrasonic Techniques for Fluid Characterization.

[33] Timothy G. Leighton 2007. What is Ultrasound?. Progress in Biophysics and Molecular Biology, 93, 3–83.

[34] Grechishkin, V. A., Perepechko 1970. I. I. Akust. Zh., 16-223.

[35] Moseley, W. W. Jr. J 1960. Appl Polymer Sci.. 3, 9-266.

[36] Matthias Messer 2005. Pulsed Ultrasonic Doppler Velocimetry for Measurement of Velocity Profiles in Small Channels and Cappilaries. Ms.D Thesis, Georgia Institute of Technology December.

[37] Pierce, A. D. 1981. Acoustics: An Introduction to Its Physical Principles and Applications. New York, Mcgraw-Hill.

[38] Volkan Köseli 2009. Experimental and Theoretical Investigation of Complex Flows by Ultrasound Doppler Velocimetry. Ph.D. Thesis.

[39] Landau, L. D. and Lifshits, E. M. 1965. The Theory of Elasticity, Moscow.

[40] Ken A. Dill 1980. Concentration Dependence of The Viscosity and Viscoelasticity of Polymer Solutions: Application of the Theory of Muthukumar And Freed. Macromolecules, 13, 620-622.

APPENDICES

A1. Derivation of Loss and Storage Modulus in Terms of Acoustic Parameters

The governing differential equation for the longitudinal sound wave propagation in elastic medium can be written as;

$$\rho \frac{\partial^2 u}{\partial t^2} = \left[K + \frac{4}{3} G \right] \frac{\partial^2 u}{\partial x^2} \qquad \text{(A1.1)}$$

Assuming that "u" is proportional with exp{iwt-xσ}, and inserting this into the equation A1.1 ;

$$V^2 = \frac{K + \frac{4}{3} G}{\rho} \qquad \text{(A1.2)}$$

where V is the longitudinal sound wave velocity in Equation A1.2. Complex modulus has already been defined in Equation 3.4 as;

$$M^* = M' + iM'' \qquad (3.4)$$

Assuming "u" is proportional with exp{iwτ-(α+iw/V)x}, the relation between M', M'' and α, V can be obtained.

Separating the imaginary and real parts of the M, it is found that;

$$M' = \frac{\rho c^2 \left[1 - \left(\frac{\alpha \lambda}{2\pi} \right)^2 \right]}{\left[1 + \left(\frac{\alpha \lambda}{2\pi} \right)^2 \right]^2} \qquad (3.2)$$

$$M'' = \frac{2\rho c^2 \frac{\alpha\lambda}{2\pi}}{\left[1+\left(\frac{\alpha\lambda}{2\pi}\right)^2\right]^2} \tag{3.3}$$

In addition the value of "$\frac{\alpha\lambda}{2\pi}$" is usually very low with respect to 1. Hence, further simplifications on the equations 3.2 and 3.3 give that;

$$M' = \rho V^2 \tag{A1.3}$$

$$M'' = \frac{2\rho V^3 \alpha}{w} \tag{A1.4}$$

A2. Obtaining the Governing Differential Equations

Considering the plane sound wave propagation in isotropic heat conducting viscoelastic medium, the equation of continuity, motion and thermal energy simplifies to;

$$\frac{\partial \rho}{\partial t} + \rho \frac{\partial v_x}{\partial x} = 0 \tag{A2.1}$$

$$\rho \frac{\partial^2 u}{\partial t^2} - \frac{\partial \sigma_{xx}}{\partial x} = 0 \tag{A2.2}$$

$$\rho C_V \frac{\partial T}{\partial t} - \frac{T\alpha_V}{\rho} K_T \frac{\partial \rho}{\partial t} = -\frac{\partial q_x}{\partial x} \tag{A2.3}$$

For the velocity of particles of the medium it can also be written that;

$$v = \frac{du}{dt} \tag{A2.4}$$

To solve the systems of differential equations simultaneously, it is essential to express the stress tensor. The stress tensor for an isotropic viscoelastic medium can be formulated as [39];

$$\bar{\sigma}_{ik} = \sigma_{ik} + \sigma_{ik}' \tag{A2.5}$$

where σ_{ik} = stress tensor of elastic solid

and σ_{ik}' = dissipative stress tensor

For the elastically deformed bodies, the stress tensor is given by

$$\sigma_{ik} = \left(\frac{\partial A}{\partial u_{ik}} \right)_T \tag{A2.6}$$

where A= Helmholtz free energy

u_{ik} = strain tensor

For small deformations strain tensor is determined by;

$$u_{ik} = \frac{1}{2}\left(\frac{\partial u_i}{\partial x_k} + \frac{\partial u_k}{\partial x_i} \right) \tag{A2.7}$$

It can also be converted into

$$u_{ik} = \left(u_{ik} - \frac{1}{3}\delta_{ik} u_{ll} \right) + \frac{1}{3}\delta_{ik} u_{ll} \tag{A2.8}$$

Helmholtz free energy as a function of temperature can be written as

$$A(T) = A_0(T) - K_T \alpha_v (T - T_0) u_{ll} + G\left(u_{ik} - \frac{1}{3}\delta_{ik} u_{ll} \right)^2 + \frac{K_T}{2} u_{ll}^2 \tag{A2.9}$$

Inserting into Equation A2.6

$$\sigma_{ik} = -K_T \alpha_V (T - T_0)\delta_{ik} + K_T u_{ll}\delta_{ik} + 2G\left(u_{ik} - \frac{1}{3}\delta_{ik} u_{ll} \right) \tag{A2.10}$$

Hence;

$$\sigma_{xx} = -K_T \alpha_V (T - T_0) + \left(K_T + \frac{4}{3}G \right) \frac{\partial u_x}{\partial x} \tag{A2.11}$$

The term $\left(K_T + \frac{4}{3}G \right)$ can also be expressed as longitudinal modulus, L.

A3. Technical Specifications of DOP2000

Technical Specifications

Emission	
Emitting Frequency	Model 2032 5 different frequencies : 0.5, 1 , 2, 4 and 8 MHz
Emitting Power	3 levels. Instantaneous maximum power for setting (approx.) : low = 0.5 W, medium = 5 W, high = 35 W
Number of emitted cycles	2, 4 or 8 cycles
Pulse Repetition Frequency	selectable values between 10000 µs and 64 µs, step of 1 µs
Reception	
Number of Gates	variables between 1000 and 3, step of 1 gate
Position of the First Channel	movable by step of 250 ns
Amplification (TGC)	Uniform, Slope, Custom Slope mode Exponential amplification between two defined depth values. Value at both depths variable between -40 dB and +40 dB Custom mode User's defined values between -40 dB and + 40 dB In cells.

	Variable number, size and position of the cells.
Sensitivity	> -100 dBm
Resolution	
Sampling Volume: lateral size	resolution defined by the acoustical characteristics of the transducer
Sampling Volume: longitudinal	
size	Model 2032
	Minimum value of 1.2 μs or 0.9 mm
	Depends on busrt length
	Maximum value of 16 μs or 12 mm
	(c = 1500 m/s, approximate value, defined at 50 % of the received)
Display Resolution	distance between the center of each sample
	Volume selectable between 0.25 μs or 0.187 mm
	and 20 μs or 15 mm, step of 0.25 μs (c =1500 m/s)
Velocity Resolution	1 LSB, doppler frequency given in a signed
	Byte format
	Maximum = 0.0091 mm/s; minimum = 91.5
	mm/s (c=1500 m/s)
Ultrasonic Processor	
Doppler Frequency	computation based on a correlation algorithm
Bandwidth of Demodulated	
Signals	Model 2032

	Bandwidth 220 kHz
Wall Filter	Stationary echoes removed by IIR high-pass
	Filter 2nd order
Number of Emissions per Profile	between 1024 and 8, any values
Detection Level	5 levels of the received Doppler energy may
	disable the computation
Acquisition Time per Profile	minimum: about 2-3 ms
Filters on profiles	moving average:
	Based on 2 to 32000 profiles
	Zero values included or rejected
	Median, based on 3 to 32 profiles
Maximum Velocity	11.72 m/s for bi-directional flow (at 0.5 MHz,
	c = 1500 m/s)
	variable positive and negative velocity range.
Acquisition	
Compute and Display	velocity
	Doppler energy
	Echo modulus
	Velocity profile with echo modulus or
	Doppler energy
	Velocity profile with velocity versus time of
	One selected gate
	Velocity profile with flow rate versus time

	(circular section assumed)
	Velocity profile with real time histogram
	Echo modulus with real time histogram
	Doppler energy with real time histogram
	Power spectrum of one selected gated
Cursor	displays the velocity and depth value, tracking
	Mode (follow the displayed curve).
	Statistical values available.
Statistics	Mean, standard deviation, minimum, maximum
Trigger	by external signal, change in the logic state
	(TTL/CMOS level)
	by keyboard action
	Selectable repeated acquisition procedure
	Of bloc of profiles
	Automatic record capability
Trigger Delay	from a 1 ms to 1s, step of 1 ms
Utilities	freeze/run mode
Velocity Component	automatic computation of the projected velocity component
Replay Mode	replays a recorded measure from the disk
Memory/Files	
Internal Memory	variable size, memorization from 2 to 32000
	Profiles
Configuration	10 saved configurations

Data File	Binary (include: ASCII short into blocks, 476 bytes Of ASCII comments, all parameters, all data Profiles) ASCII (statistical information available)

A4. The Raw Data Obtained From the Rheological Characterization of CMC/Water Solutions

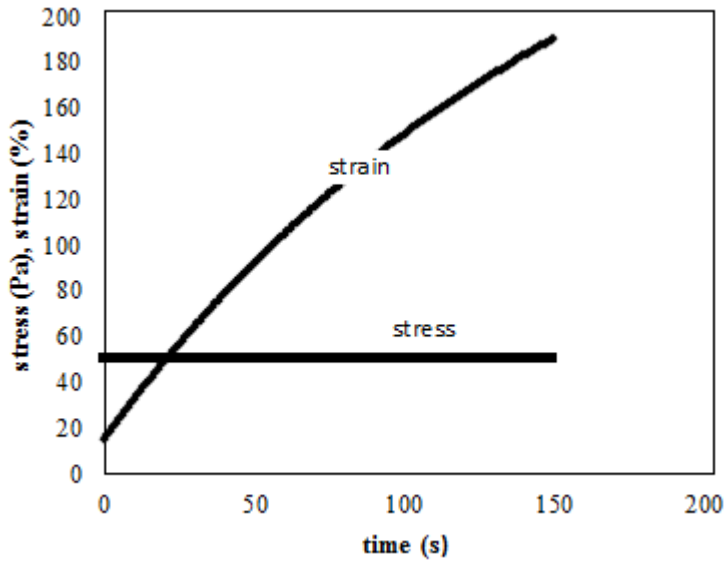

Figure A.4.1 Results of the creep experiment on 2.0 wt. % CMC solution

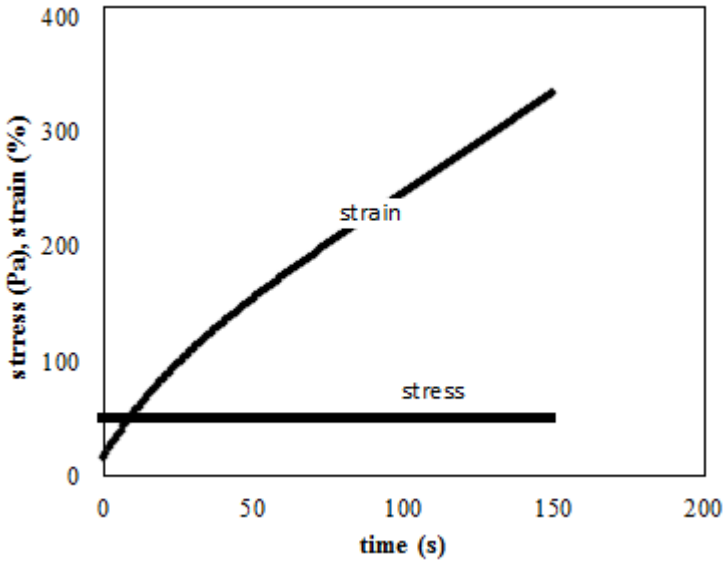

Figure A.4.2 Results of the creep experiment on 3.0 wt. % CMC solution

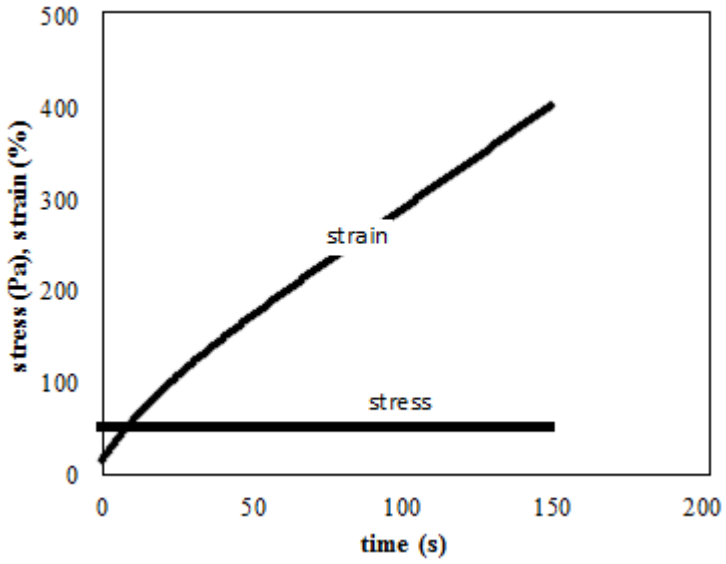

Figure A.4.3 Results of the creep experiment on 4.0 wt. % CMC solution